



HAL
open science

BATAL: The Balloon measurement campaigns of the Asian Tropopause Aerosol Layer

J.-P. Vernier, T. D. Fairlie, T. Deshler, M. Venkat Ratnam, H. Gadhavi, M. Natarajan, A. K. Pandit, A Raj, A. H. Kumar, A. Jayaraman, et al.

► **To cite this version:**

J.-P. Vernier, T. D. Fairlie, T. Deshler, M. Venkat Ratnam, H. Gadhavi, et al.. BATAL: The Balloon measurement campaigns of the Asian Tropopause Aerosol Layer. *Bulletin of the American Meteorological Society*, 2018, 99 (5), pp.955-973. 10.1175/BAMS-D-17-0014.1 . insu-01799122

HAL Id: insu-01799122

<https://insu.hal.science/insu-01799122>

Submitted on 24 May 2018

HAL is a multi-disciplinary open access archive for the deposit and dissemination of scientific research documents, whether they are published or not. The documents may come from teaching and research institutions in France or abroad, or from public or private research centers.

L'archive ouverte pluridisciplinaire **HAL**, est destinée au dépôt et à la diffusion de documents scientifiques de niveau recherche, publiés ou non, émanant des établissements d'enseignement et de recherche français ou étrangers, des laboratoires publics ou privés.



AMERICAN METEOROLOGICAL SOCIETY

Bulletin of the American Meteorological Society

EARLY ONLINE RELEASE

This is a preliminary PDF of the author-produced manuscript that has been peer-reviewed and accepted for publication. Since it is being posted so soon after acceptance, it has not yet been copyedited, formatted, or processed by AMS Publications. This preliminary version of the manuscript may be downloaded, distributed, and cited, but please be aware that there will be visual differences and possibly some content differences between this version and the final published version.

The DOI for this manuscript is doi: 10.1175/BAMS-D-17-0014.1

The final published version of this manuscript will replace the preliminary version at the above DOI once it is available.

If you would like to cite this EOR in a separate work, please use the following full citation:

Vernier, J., T. Fairlie, T. Deshler, M. Ratnam, H. Gadhavi, S. Kumar, M. Natarajan, A. Pandit, A. Raj, H. Kumar, A. Jayaraman, A. Singh, N. Rastogi, P. Sinha, S. Kumar, S. Tiwari, T. Wegner, N. Baker, D. Vignelles, G. Stenchikov, I. Shevchenko, J. Smith, K. Bedka, A. Kesarkar, V. Singh, J. Bhate, V. Ravikiran, M. Rao, R. Babu, A. Patel, H. Vernier, F. Wienhold, H. Liu, T. Knepp, L. Thomason, J. Crawford, L. Ziemba, J. Moore, S. Crumeyrolle, M. Williamson, G. Berthet, F. Jegou, and J. Renard, 2017: BATAL: The Balloon measurement campaigns of the Asian Tropopause Aerosol Layer. *Bull. Amer. Meteor. Soc.* doi:10.1175/BAMS-D-17-0014.1, in press.



1 **BATAL: The Balloon measurement campaigns of the Asian Tropopause Aerosol Layer**

2

3 A series of NASA/ISRO-sponsored balloon campaigns in India and Saudi-Arabia between
4 2014 and 2017 to study the nature, formation and transport of polluted aerosols in the Upper
5 Troposphere and Lower Stratosphere during the Asian Summer Monsoon.

6

7 *J.-P. Vernier^{1,2}, T.D. Fairlie², T. Deshler³, M. Venkat. Ratnam⁴, H. Gadhavi^{4*}, S. Kumar⁵, M.*

8 *Natarajan², A.K. Pandit^{4*}, Akhil Raj S. T. ⁴, A. H. Kumar⁴, A. Jayaraman⁴, A. K. Singh⁶, N.*

9 *Rastogi⁷, P.R. Sinha⁵, S. Kumar^{6#}, S. Tiwari⁶, T. Wegner², N. Baker², D. Vignelles⁸, G.*

10 *Stenchikov⁹, I. Shevchenko⁹, J. Smith¹⁰, K. Bedka², A. Kesarkar⁴, V. Singh⁴, J. Bhate⁴, V.*

11 *Ravikiran⁴, M.D. Rao⁴, S. Ravindrababu⁴, A. Patel⁷, H. Vernier¹³, F. G. Wienhold¹¹, H. Liu¹⁴,*

12 *T. Knepp^{1,2}, L. Thomason², J. Crawford², L. Ziemba², J. Moore¹, S. Crumeyrolle¹², M.*

13 *Williamson¹⁰, G. Berthel⁸, F. Jégou⁸, J.B. Renard⁸.*

14

15 1. Science Systems and Applications, Inc., USA

16 2. NASA Langley Research Center, USA

17 3. University of Wyoming, Laramie, USA

18 4. National Atmospheric Research Laboratory, Gadanki, India

19 5. TIFR Balloon Facility, Hyderabad, India

20 6. Banaras Hindu University, Varanasi, India

21 7. Physical Research Laboratory, Ahmedabad, India

22 8. LPC2E/CNRS/University of Orléans, 3A Avenue de la recherche scientifique, Orléans,

23 France.

24 9. King Abdullah University of Science and Tech., Saudi Arabia

25 10. Smith and Williamson, Inc., USA

- 1 11. Swiss Federal Institute of Tech., Zurich, Switzerland
- 2 12. LOA, CNRS–Université Lille1, Villeneuve d’Ascq, France
- 3 13. Virginia Institute of Marine Science, Gloucester, USA.
- 4 14. National Institute of Aerospace, Hampton, VA, USA

5

6 * Now at Physical Research Laboratory, Ahmedabad, India.

7 # Now at Aryabhata Research Institute of Observational Sciences (ARIES), Manora Peak,
8 Nainital, India.

9

10 Corresponding author :

11 Jean-Paul Vernier

12 Science Systems and Applications, Inc.

13 NASA Langley Research Center

14 Hampton, VA, USA

15 jeanpaul.vernier@nasa.gov

16

17

18

19

20

21

22

23

24

25

1 **Abstract**

2

3 We describe and show results from a series of field campaigns using balloon-borne
4 instruments launched from India and Saudi Arabia during the summers 2014-2017 to study
5 the nature, formation and impacts of the Asian Tropopause Aerosol Layer (ATAL). The
6 campaign goals were to i) characterize the optical, physical and chemical properties of the
7 ATAL, ii) assess its impacts on water vapor and ozone, and iii) understand the role of
8 convection in its formation. In order to address these objectives, we launched 68 balloons
9 from 4 locations, one in Saudi-Arabia and 3 in India, with payload weights ranging from 1.5
10 kg to 50 kg. We measured meteorological parameters, ozone, water vapor, and aerosol
11 backscatter, concentration, volatility and composition in the Upper Troposphere and Lower
12 Stratosphere (UTLS) region. We found peaks in aerosol concentrations of up to 25 part/cm^3
13 for radius $> 75 \text{ nm}$, associated with Scattering Ratio at 940 nm of ~ 1.9 near the cold point
14 tropopause. During medium-duration balloon flights near the tropopause, we collected
15 aerosols and found, after offline ion chromatography analysis, the dominant presence of
16 nitrate ions with a concentration of about 100 ng/m^3 . Deep convection was found to influence
17 aerosol loadings 1 km above the cold point tropopause. The BATAL project will continue for
18 the next 3-4 years and the results gathered will be used to formulate a future NASA-ISRO
19 airborne campaign with NASA high altitude aircraft.

20

21

22

23

24

25

1 **I. Introduction.**

2
3 Asian pollution sources and their strength have changed over the last few decades.
4 Recent satellite observations have shown that the highest NO₂ and SO₂ emissions have
5 shifted from China to India (Krotkov et al., 2016). China's SO₂ emissions have decreased by
6 50% after the installation of desulfurization system in their power plants, while SO₂
7 emissions in India have doubled between 2005 and 2015 (Krotkov et al., 2016). The shift in
8 the highest SO₂ emissions toward the tropics could have serious implications for their
9 redistribution in the atmosphere. During the Asian Summer Monsoon (ASM), tropical
10 convective systems provide a vertical transport pathway for boundary layer pollutants to
11 reach the Tropical Tropopause Layer (TTL), which is a gateway to the global stratosphere.
12 SO₂ and other gas-phase precursors transported into the TTL can be converted into sulfuric
13 acid droplets and other aerosols with consequences for the radiative balance, stratospheric
14 ozone chemistry, and the properties of cirrus clouds near the tropopause (Kremser et al.,
15 2016).

16 Satellite observations have revealed the presence of pollution markers (e.g., CO,
17 HCN, CH₄) in the UTLS region during the ASM (Park et al., 2007; Randel et al., 2006,
18 2010). Together with model simulations (e.g., Lawrence et al., 2010), these studies suggest
19 that deep convection can serve as a conduit for the transport of gas-phase boundary-layer
20 pollutants to the UTLS. Pollutants can accumulate in the UTLS under anticyclonic flow
21 conditions (the Asian anticyclone) which characterize the UTLS between the Eastern
22 Mediterranean Sea and China during the ASM, and which encompasses Northern India.
23 Figure 1 shows a sketch of the transport mechanisms associated with the ASM. An overpass
24 of the CALIPSO (Cloud-Aerosol Lidar and Infrared Pathfinder Satellite Observations) lidar
25 for August, 12th 2017 shows the vertical extension of convective storms reaching the UTLS

1 over India. Air transported via the ASM anticyclone to the tropical upper troposphere can
2 reach the lower stratosphere via relatively slow diabatic ascent (Garny and Randel, 2016). In
3 addition, strong Mesoscale Convective Systems (MCSs) in India can directly penetrate the
4 lower stratosphere. Detrainment of air from the anticyclone due to transience in the flanking
5 jet streams, in particular Rossby-wave breaking along the subtropical jet can lead to
6 irreversible exchange of air with the extratropical lower stratosphere (Vogel et al., 2016),
7 with implications for the lower stratospheric composition throughout the hemisphere.

8 In addition to trace gases, aerosol concentrations are enhanced in the UTLS during the
9 ASM. CALIPSO satellite observations have shown a recurrent aerosol layer in clear-sky
10 summertime backscatter profiles near 13-18 km from the Eastern Mediterranean Sea to
11 Western China and India (Vernier et al., 2011, 2015), called the Asian Tropopause Aerosol
12 Layer (ATAL). The ATAL was confirmed through solar occultation observations by
13 Stratospheric Aerosol and Gas Experiment (SAGE) II (Thomason and Vernier, 2013) after
14 improving the cloud-aerosol separation approach using the ratio between aerosol extinction
15 coefficients retrieved at two wavelengths. Analysis of long-term satellite measurements of
16 UTLS aerosols suggests that ATAL's aerosol optical depth has increased by 2-3 times since
17 the late 1990's pointing out its possible connection with Asian pollution growth (Vernier et
18 al., 2015). Satellite observations of ATAL are consistent with early measurements carried out
19 from the Tibetan plateau during the late 90's. Ground based lidar in Lhasa (Tibet, China),
20 showed the presence of an aerosol layer between 14–19 km with $SR = 1.1-1.2$ and $\delta < 5\%$
21 (Kim et al., 2003). In addition, balloon measurements at the same location in August 1999
22 have shown an enhancement of small particles of effective radius $< 0.6\mu\text{m}$ near the tropopause
23 (Tobo et al., 2007). More recently, in situ backscatter measurements using the Compact
24 Optical Backscatter Aerosol Detector (COBALD) and aerosol size distribution from the

1 Printed Optical Particle Spectrometer (POPS) have confirmed the presence of the ATAL
2 (Vernier et al., 2015, Yu et al., 2017).

3 The presence of aerosol near the tropopause could impact the Earth's radiative
4 balance, and the properties of cirrus clouds. The direct summertime radiative forcing
5 resulting from the AOD increase of the ATAL, since the late 1990s, was estimated near -0.1
6 W/m² using radiative parameters corresponding to sulfate aerosol. This represents 1/3 of the
7 total radiative forcing due to increased CO₂ over the same period (Vernier et al., 2015). Thus,
8 the ATAL appears to be a significant player in the Earth's radiative budget of the Northern
9 Hemisphere at decadal scale. Aerosol near the tropopause can potentially affect stratospheric
10 ozone. Solomon et al. (2016) suggested that heterogeneous chlorine chemistry occurring on
11 aerosol in the lower stratosphere during the ASM could impact the local budget and long-
12 term trend of ozone in the UTLS. Finally, the presence of aerosol near the tropopause can
13 potentially alter the properties of TTL cirrus clouds. Pandit et al. (2015) showed that the
14 frequency of sub-visible cirrus (SVC) in South India has increased by 9% from 1998-2013,
15 with possible connections with the positive trend in ATAL's AOD since the late 90's
16 (Vernier et al., 2015).

17 Since 2014, we have organized a series of balloon field campaigns in India and Saudi-
18 Arabia during the ASM to better understand the nature, formation, and impacts of the ATAL.
19 We chose 3 balloon sites in India to sample air masses directly influenced by convection and
20 to capture the horizontal gradient of aerosol in the UTLS region from the edge to the center
21 of the ASM Anticyclone. The location in Saudi Arabia was selected for measurements
22 downwind from the monsoon region and study the evolution of air masses along their
23 transport.

24

25

1 The BATAL campaigns specifically address the following science questions:

2 I. What are the optical properties, size distribution and composition of the ATAL ?

3 II. How do ozone and water vapor behave near the ATAL?

4 III. How does convection affect the ATAL

5
6 **II. Description of the BATAL campaigns.**

7
8 The BATAL campaigns have comprised a total of ~68 balloon flights between 2014-
9 2017 from India and Saudi Arabia, with payload weights ranging from 1.5 kg to 50 kg. The
10 effort has involved a number of institutes from the United States (Science Systems and
11 Applications, Inc., NASA Langley Research Center, and University of Wyoming), France
12 (LPC2E/CNRS/University of Orléans), Switzerland (Swiss Federal Institute of Tech.), Saudi-
13 Arabia (King Abdullah University of Science and Technology: KAUST), and India (National
14 Atmospheric Research Laboratory: NARL, Tata Institute of Fundamental Research: TIFR,
15 Banaras Hindu University: BHU, Physical Research Laboratory: PRL). Figure 2 shows the
16 position of the launch sites (Gadanki, Hyderabad, Varanasi and Thuwal) and the trajectories
17 of the balloon flights conducted during the campaigns. Most of the time, the balloons drifted
18 westward in strong easterly winds of up to 40 m/s near the cold point tropopause. Most of the
19 payloads launched from India were recovered after landing within 300 km from the launch
20 site while most of the balloon flights from Thuwal (Saudi Arabia) landed in the Red Sea.

1 a. Ballooning during BATAL.

2 We used different balloon platforms (Table 1, Figure 3) over the 4-year BATAL effort to
3 address the science questions described in section 1:

- 4 - **HF:** The characterization of the optical and physical properties of the ATAL is addressed
5 with aerosol payloads onboard Heavy balloon Flights (HFs) with total payload weight
6 greater than 30 kg using 3000 m³ polyethylene balloons. HFs took place from the TIFR
7 balloon facility, Hyderabad (India), in August 2015 and 2017. The balloon facility
8 manufactured the balloons and provided the logistical support for the launches and the
9 recovery of the payloads. During those flights, we also studied the behavior of the ozone
10 and water vapor near the ATAL.
- 11 - **ZF:** The chemical composition of the ATAL has been studied using an aerosol impactor
12 onboard balloon flights floating near the tropopause for several hours, called Zero-
13 pressure Flights (ZF). The float duration was critical to collect a sufficient concentration
14 of aerosols on the filters mounted on the aerosol impactor. Filters were sent post-flight
15 for Ion Chromatrography (IC) analysis within 12 hours after launch. 4 ZF flights were
16 conducted from TIFR since 2015. The time evolution of the GPS altitude of those flights
17 is shown in Fig. 5. The first flight (ZF0) in 2016 did not have a ballast module and the
18 floating duration between 14 and 18 km was only 50 min. In 2017, we conducted three
19 additional balloon flights and each one of them included ballast module. The maximum
20 floating duration above 14 km of 2h 50 min was achieved during ZF3.

ZF : A New concept for TTL measurements

In order to achieve extended flotation in the UTLS, the Zero-pressure Flights (ZF), included a ballast module to compensate for altitude loss due to extremely cold temperature near the tropopause. Figure 4 shows a sketch of the Static Launch Method (SLM) used for the ZFs at the balloon facility of TIFR. During the launch preparation, the plastic balloon is fully deployed and the top portion of it is blocked under a small aluminum roller mounted on the top of a trolley for initial balloon inflation. The bottom part of the balloon is connected to the flight train with the parachute, the communication device and the science payloads. The ballast module, the last element of the flight train, is hooked to a vehicle. Tow balloons (launch balloons of 20 kg lift capacity) are tied to the communication payload to lift the load line into the air. During the inflation of balloon, adequate tension is taken by moving the vehicle forward or backward. During the launch, the balloon is released first from the roller until the load line becomes vertical. At that time, the anchor nylon rope between the ballast module and vehicle is cut. Immediately after releasing the payload, a telecommand is given to separate the tow balloons.

- **LF/MF:** The optical properties of the ATAL were studied using a backscatter sonde, called COBALD (Compact Optical Backscatter Aerosol Detector) flown under a meteorological sonde for Light Flights (LF) with 1200 g latex balloons and a total payload weight of less than 1.3 kg. Medium Flights (MF) included, in addition to LF payloads, ozone and water vapor sensors, and sometimes a light-weight aerosol counter to study the size distribution of the ATAL and the chemical composition of the UTLS.
- **BF:** In order to study the influence of convection on the ATAL, we used a controlled balloon system, developed by Smith and Williamson, Inc., called Boomerang. The

1 rational was to have a flexible and simple system to launch payloads of less than 10 kg in
2 weather conditions which would not be possible for ZF or HF flights. The goal was to
3 extend the measurement duration in the UTLS region and attempt to fly in convective
4 storms. Boomerang was used with a 3000g balloon and a secondary balloon (1200g) to
5 which was attached with a pressure sensitive cut down device (Doongara). The
6 secondary balloon was cut at a given altitude to rapidly slow down the ascent rate. The
7 two Boomerang flights conducted from Varanasi in August 2016 included an aerosol
8 impactor and COBALD.

Boomerang

Boomerang is a radio-controlled balloon system which includes a valve and a ballast module. The valve allows venting of helium gas from inside the balloon, controlling the internal pressure, reducing the buoyancy force and thus the ascent rate. A ballast module comprises sand which can be released to make the system lighter, increasing the balloon ascent rate.

b. Payloads.

19 In order to characterize the optical, physical and chemical properties of the ATAL,
20 we launched payloads specifically designed for aerosol measurements; these included an
21 optically based instrument to measure aerosol backscatter properties (COBALD: Compact
22 Optical Backscatter Aerosol Detector), and Optical Particle Counters (OPC) from the
23 University of Wyoming, NASA Langley and LPC2E for aerosol size distribution and
24 volatility. In addition, we launched an aerosol impactor for composition assessment. Those
25 payloads are further described below and summarized in table 3.

1 i) Aerosol measurements.

2
3 **COBALD** (Compact Optical Backscatter Aerosol Detector)

4 COBALD is a light-weight (540 g) instrument which consists of two high-power
5 LEDs that emit about 250 mW optical power each at wavelengths of 455 and 940 nm,
6 respectively. The backscattered light from the molecules, aerosols, or ice particles is recorded
7 by a silicon photodiode using phase-sensitive detection. The backscatter ratio between
8 aerosols and molecules is inferred from the signal using the radiosonde air pressure and
9 temperature to calculate the molecular backscatter. This ratio is not quantified absolutely, but
10 the analysis of the entire sounding profile imposes physical constraints such that it is confined
11 to an absolute error interval of 5%, while precision along the profile is better than 1% in the
12 UTLS region (Vernier et al., 2015). We use the Color Index (CI), the ratio between SR-1 at
13 940 nm and 455 nm to eliminate ice clouds in the COBALD data. The COBALD data are
14 usually calibrated in the upper stratosphere above 30 km in the quasi-absence of aerosols.

15
16 **University of Wyoming OPC (Wyo)**

17 The Optical Particle Counter (OPC) flown by the University of Wyoming (Deshler et
18 al., 2003) provides vertical profiles of size-resolved aerosol concentration at 8 radii between
19 0.075 and 15 μm . A second OPC with an inlet heated to 180°C was included to determine the
20 non-volatile fraction of aerosol concentration. In addition, a Condensation Nuclei (CN)
21 counter was added to the OPCs to measure the total aerosol number concentration (Campbell
22 and Deshler, 2014).

1 **Langley OPC (Lan)**

2 A small balloon-borne OPC payload was developed based upon the adaptation of the
3 MetOne OPC profiler to make aerosol concentration measurement in 8 radii between 0.15 to 5
4 micron up to the middle stratosphere. Flow and electronic systems are adapted for balloon
5 flight application and data are transmitted through an iMet radiosonde (Vernier et al., 2017, in
6 preparation).

7

8 **Balloon-borne Aerosol Impactor (BAI)**

9 To assess the composition of UTLS aerosols, a Balloon-borne Aerosol Impactor (BAI)
10 was developed. A ground-based impactor was attached to a scroll pump and controlled by an
11 electronic board based upon meteorological and GPS data from an iMet radiosonde. The pump
12 was switched on and off at the desired pressure to collect aerosols in a given altitude range. We
13 used a 4-stage aerosol impactor from *California Measurement Inc.* with cutoff radius of 0.025,
14 0.075, 0.25 and 1 μm at a flow of 7 lpm (liter per minute).

15

16 **LOAC**

17 LOAC (Light Optical Aerosol Counter) is a miniature OPC (Renard et al., 2016). It
18 contains a laser (650 nm) and measures the intensity of the light scattered at two angles 12°
19 and 60° (Lurton et al. 2014). The particle number concentration is provided over 19 size classes
20 from 0.1 to 50 μm in radius at sampling interval of 1 min. Uncertainties are estimated to be of
21 $\pm 30\%$ for smaller size bins (Renard et al., 2016). In addition to number concentration, the
22 LOAC gives a specific index relative to the main optical nature of the aerosol sampled, called
23 typology, which is obtained by combining the intensities of light at two scattering angles
24 (Renard et al. 2016). Typology is calibrated in laboratory with response given by known
25 samples. Three LOAC OPCs were launched from Varanasi during BATAL 2015. The first two

1 LOAC instruments flown using MF balloons together with a CFH, a Lan OPC, and an
2 ozonesonde did not reached ATAL altitudes. The third LOAC instrument launched in a LF
3 configuration reached the lower stratosphere. No significant enhancement in the aerosol
4 content was detected in the tropopause region possibly due to the regular losses of telemetry
5 encountered at these altitude levels.

6

7 ii) Temperature, pressure, ozone and water vaport measurements.

8

9 Ozone and water vapor concentration measurements accompanied aerosol
10 observations on a number of occasions to study the behavior of the ATAL and UTLS
11 chemistry, using an ozonesonde and a Cryogenic Frost Point Hygrometer (CFH),
12 respectively. We used iMet radiosondes onboard most of the balloon flights, and occasionally
13 a Meisei (RS-11G) radiosonde, to transmit data, follow the balloon trajectory, and obtain the
14 landing location. We included SPOT and GSM based locators on most of the flights to
15 determine the exact location of the landing and improve the chance of recovery.

16 **Radiosondes**

17 We used Meisei (RS-11G) and iMet radiosondes. These instruments measure
18 temperature from -90°C to 50°C with resolution of 0.1°C and accuracy of 0.5°C. ~~Wind speed~~
19 ~~resolution is 0.1m/s with an accuracy of 0.2 m/s.~~ Further details of this radiosonde system, data
20 base and quality checks applied to the data are reported by Venkat Ratnam et al. (2014).

21

22 **Ozonesondes**

23 We launched Electrochemical Concentration Cell (ECC) Ozonesondes (Komhyr et al.,
24 1995) to measure the vertical distribution of ozone from the surface to balloon burst altitude.
25 The measurement is based on electrochemical oxidation of potassium iodide by ozone in

1 aqueous solution. The accuracy of the ECC Ozonesonde is ~5 – 10%. More details of the
2 ozonesondes being used at NARL in Gadanki is provided by Akhil Raj et al. (2015).

3

4 **Cryogenic Frost point Hygrometer (CFH)**

5 The CFH measures water vapor concentration through the chilled-mirror principle
6 using a cryogenic liquid as a coolant. A small mirror attached at the end of the cold finger piece
7 is electrically heated and cryogenically cooled to maintain a constant thin layer of frost that is
8 optically detected. The mirror temperature is then equal to the ambient dew point or frost point
9 temperature and is measured by a small thermistor embedded in the surface of the mirror. The
10 frost-point temperature is used to calculate the partial pressure of water vapor in air (Goff and
11 Gratch, 1946) and determine the water vapour mixing ratio (WVMR) with an uncertainty of
12 about 4% in the lower tropical troposphere to about 10% in the middle stratosphere and tropical
13 tropopause (Vömel et al., 2007).

14

15 d. Ground-based and modelling support.

16 i. Ground-based support

17 Throughout the campaign at the National Atmospheric Research Laboratory (Gadanki)
18 and at the King Abdulah University for Science and Technology (Thuwal), observations were
19 available from additional instrumentations, listed in Table 4. These include ground-based lidar
20 observations which can be compared with COBALD in-situ backscatter measurements from
21 the boundary-layer to the middle stratosphere and can be used to validate CALIPSO satellite
22 aerosol retrievals. A current project at KAUST uses COBALD/AERONET and MPL
23 measurements to help characterize the vertical and temporal structures of dust in the Boundary
24 Layer. Ground-based lidar measurements from Gadanki are used to characterize the ATAL and
25 sub-visible cirrus clouds near the tropopause. In addition, the MST radar from Gadanki can

1 help assess the influence of convection on the balloon measurements. All ground-based support
2 during the BATAL campaigns provided quasi-collocated observations with the balloon-borne
3 measurements to better characterize the vertical structure and properties of aerosols and clouds.

4

5 ii. Modelling support.

6

7 Throughout the BATAL campaign in India weather forecasts
8 (<http://forecast.narl.gov.in/weather>) provided by NARL and near-real time Doppler weather
9 radar images obtained from Indian Meteorological Department
10 (<http://www.imd.gov.in/section/dwr/dynamic/dwr.htm>) supported flight planning for balloon
11 launches.

12 Starting with the 2017 campaign, regional and global chemical transport simulations have
13 been carried out using Weather Research and Forecasting (WRF) model coupled with
14 chemistry (WRF-Chem), version 3.6.1, and the NASA Goddard Earth Observing System
15 (GEOS), version 5, (<https://gmao.gsfc.nasa.gov/forecasts/>) with chemical and aerosol forecasts
16 over South Asia.

17 WRF-Chem was run with a horizontal resolution of 27 km and 30 vertical levels from the
18 ground to 50 hPa. Meteorological initialization and boundary conditions were derived from the
19 NCEP-GFS data available every six hours. Anthropogenic emissions have been obtained from
20 HTAP-EDGAR (Janssens-Maenhout et al., 2015) that contains the annual anthropogenic
21 emissions of greenhouse gases and air pollutants at 0.1x0.1 degree spatial resolution. The
22 simulations have been carried out with the MOZCART gas-phase chemistry (Emmons et al.,
23 2010) and GOCART aerosols (Chin, 2002).

24 The GEOS "Forward Processing" (FP) system generate weather analysis, assimilation
25 products, and 10-day weather and composition forecasts

1 (https://gmao.gsfc.nasa.gov/weather_prediction/). The forecasted fields used for the BATAL
2 campaign included U and V winds, water vapor, cloud fraction, ozone, carbon monoxide (CO),
3 sulfur dioxide (SO₂), column aerosol optical depths, and aerosol coefficients. Figure 6 shows
4 maps of carbon monoxide (CO), sulfate, nitrate, and black carbon (BC) concentrations at 100 hPa
5 for 21 UTC, August 3, 2017, as predicted by NASA GEOS-5 on July 30, 2017 at 00 UTC. High levels
6 of CO in the upper troposphere forecasted over Gadanki during BATAL 2017
7 likely resulted from the convective transport of polluted air from eastern China followed by
8 westward transport along the southern edge of the Asian Anticyclone. Sulfate and black carbon
9 aerosol layers were also approaching South India at that time. We used forecasts to make the
10 necessary logistical arrangements and plan balloon flights ahead of time.

11

12 **III. Science Highlights.**

13

14 1. Characterization of the optical, physical and chemical properties of the ATAL.

15

16 a. Backscatter measurements from CALIOP and COBALD.

17

18 One of the main science objectives of the BATAL campaigns was to characterize the
19 optical properties of the ATAL at multiple locations within the Asian Anticyclone through
20 backscatter measurements using the COBALD backscatter sonde and to compare those
21 measurements with the Cloud-Aerosol Lidar and Orthogonal Polarization (CALIOP) onboard
22 CALIPSO. Three locations were selected in India to study the aerosol gradient from the
23 southern edge (Gadanki) to the interior (Varanasi) of the Asian Anticyclone. In addition, we
24 also chose one site in Saudi Arabia (Thuwal) to sample the outflow from the Indian monsoon
25 through the westward circulation prevailing in the UTLS. Figure 7 shows a map of Scattering

1 Ratio (SR) at 532 nm, optically equivalent to an aerosol mixing ratio, averaged from
2 CALIOP observations acquired between July and August 2015. Corresponding cross-sections
3 averaged between 15-45°N latitudes (bottom) and 5-105°E longitudes (right) illustrate the 3-
4 D distribution of the UTLS aerosols.

5 We used the version 4 of the CALIOP level 1 data which are based upon a new
6 calibration scheme of the nighttime profiles between 36-39 km (Vernier et al., 2009). The SR
7 is calculated from the averaged total attenuated backscatter at 532 nm every 1 degree along
8 each orbit track and corrected from ozone absorption and molecular scattering using air
9 density from the NASA GEOS-5 assimilated dataset. The data have been cleared from clouds
10 when at least 3 of 5 consecutive vertical bins have depolarization ratio values greater than 5
11 % below 20 km. All data below clouds are removed to avoid cloud attenuation effects.
12 Rogers et al. (2011) showed that the error at mid-latitudes of the CALIOP data is near 5%
13 compared to aircraft high spectral resolution lidar measurements. We anticipate that the
14 residual error from aerosol contamination in the calibration region of 36-39 km is near 2% in
15 the tropics. Thus, the total relative error on the CALIOP SR is expected to be less than 6%.
16 The ATAL is seen in Fig. 7 through elevated mean SR near 1.13 ± 0.07 from the Eastern
17 Mediterranean Sea to Western China between 360-440 K potential temperature surfaces. The
18 aerosol layer is thinner near the equator and about 3-4 km thick between 30-40°N.
19 The CALIOP and corresponding COBALD profiles obtained during the BATAL balloon
20 flights are shown in Fig.8. We use the Color Index (CI), i.e., the ratio between SR-1 at 940
21 nm and 455 nm, to eliminate ice clouds in the COBALD data. We relax the threshold on the
22 CI to 10 since the value of 7 proposed by Vernier et al. (2015) seems to remove clear sky
23 data. After visual inspection, we find that the new filter does not retain sub-visible cirrus
24 clouds.

1 The satellite and in situ measurements agree within ~10% from 14 and 24 km for the flights
2 at Gadanki and Hyderabad (Fig.8, left). The averaged profile from Thuwal (Fig.8, right)
3 exhibits a larger difference compared to CALIOP with an apparent offset of 0.3-0.4. The
4 retrievals of COBALD and CALIOP SR profiles are based upon independent calibration
5 procedures which are usually applied in the upper stratosphere. However, since the bursting
6 altitude of a balloon flight is usually below 34 km, COBALD profiles are referenced below
7 this level while CALIOP backscatter profiles are calibrated between 36 and 39 km. The
8 COBALD profiles are artificially compensated for the presence of aerosol in the calibration
9 region by multiplying by a correction factor. Differences in the calibration procedure are
10 therefore the likely cause of the differences observed at Thuwal between COBALD and
11 CALIOP.

12 Nevertheless, the ATAL is seen in both balloon and satellite profiles within the coldest region
13 of the atmosphere between 14-19 km. CALIOP observations show the absence of an ATAL
14 during the winter season (Figure 2; Vernier et al., 2015). Throughout the BATAL campaigns
15 in India, SR maxima were often located near the cold point tropopause, suggesting the
16 influence of temperature on the processes involved in aerosol formation and/or growth.

17

18 b. Advanced microphysical properties of the ATAL.

19

20 During BATAL 2015, we conducted two heavy balloon flights, carrying ~50 kg of
21 instrumentation, telecommunication, and recovery systems from the TIFR balloon facility,
22 Hyderabad (India). These balloons carried two OPCs of the University of Wyoming, one with
23 an ambient inlet and another with an inlet heated to temperature $> 180^{\circ}\text{C}$ to derive the aerosol
24 volatility fraction. In addition, a Condensation Nuclei (CN) counter from the University of
25 Wyoming was included to derive the concentration of particles with radii greater than 10 nm.
26 Figure 9 shows data from the balloon flight on August 13rd. We found a relatively high

1 concentration of aerosol (up to ~ 25 part/cm³) near the tropopause (16-19 km) with $r > 0.075$
2 μm , comparable to those observed in the boundary layer. Particle number concentration for r
3 > 0.15 and $r > 0.25$ μm is smaller by a factor of 30 and 300, respectively. The volatility
4 fraction, defined for a particular size as the difference between the unheated and heated
5 number concentration divided by the unheated concentration, shows that 80-95 % of these
6 aerosols have a volatile component, thus likely partially or totally liquid in the 16-18 km
7 altitude range. The volatile fraction of aerosol at 0.075 μm is shown in Figure 9B. The shapes
8 of the total/non-volatile aerosol concentration profiles are very similar with a peak near the
9 cold point tropopause (Fig.9B), suggesting that aerosols with a non-evaporating, and thus
10 likely solid, core had been transported at those levels. The CN measurements were saturated
11 throughout the troposphere and decreased sharply near the tropopause (Fig.9A). High aerosol
12 concentrations near the tropopause coincide with a peak in SR (~ 17 km) of 1.9 associated
13 with low Color Index (CI <10) values measured by COBALD in contrast with ice clouds
14 showing CI near 20 (15-16.5km) (Fig.9D).

15

16 c. Ozone and water vapor behavior near the ATAL.

17

18 In addition to the aerosol measurements described above, we also flew an ozonesonde
19 and a CFH for ozone and water vapor measurements, respectively. Interestingly, enhanced
20 water vapor (up to 7-8ppmv) near 17-18 km were observed just above the cold point
21 tropopause and the peak in aerosol concentration (Fig.9C and 9A). The ozone partial pressure
22 profile shown in Fig.9C displays a sharp increase from 0 to 2 mPa between 17 and 18 km.
23 The presence of a moist layer near the tropopause strongly suggests the influence of
24 convection up to these levels. Deep convection is also known to inject tropospheric air with
25 low ozone concentrations which could explain the very low ozone values near the cold point

1 tropopause. In addition, heterogenous ozone chemistry in the lower stratosphere could also
2 result in ozone depletion through chlorine activation on aerosol (Solomon et al., 2016). Thus,
3 the behavior of ozone, water vapor and aerosol can be strongly inter-related via the influence
4 of deep convection.

5

6 d. Composition of the ATAL

7

8 In order to study the composition of the ATAL, we developed a Balloon-borne Aerosol
9 Impactor (BAI, section IIb) to collect size-segregated aerosols on filters near the tropopause
10 and analyze their composition through Ion Chromatography (IC). The BAI flew on 3 ZF
11 flights on August 8th, 15th and 21st at TIFR. The pump, connected to a 4-stage impactor, was
12 switched on automatically below 150 hPa (~14 km) and above 70 hpa (~20 km). In order to
13 collect sufficient particles on filters, we maximized the floating duration of the balloons near
14 the tropopause using the ZF concept (see section II). During those flights, the pump was on
15 for 1h 20min on ZF1, 1h 47min on ZF2 and 2h 47min on ZF3. The volume of air passing
16 through the impactor was controlled and calculated with a mass flow meter. A total volume
17 of 566 L and 917 L of air was sampled during ZF2 and ZF3, respectively. In addition, the
18 BAI was run on the roof top of TIFR balloon facility on August 23rd for 45 min to provide a
19 comparison basis for the flight measurements. After 3 succesfull ZF flights, the BAI was
20 recovered in good condition and brought back to TIFR. The filters were loaded and unloaded
21 from the BAI in a clean room of class 7 and refrigerated at -24°C. The filters were transported
22 from TIFR to the Physical Research Laboratory in Ahmedabad by flight using a cooler with
23 dry ice to maintain temperature at freezing levels. Figure 10 shows the concentration of ions
24 measured through IC at the Physical Research Laboratory in Ahmedabad. We note the
25 presence of nitrate ions with a concentration about 100 ng/m³ on ZF2 and ZF3, nearly 6 times

1 smaller than ground levels. Traceable amount of Calcium ions were also observed on both
2 ZF2 and ZF3 filters. We note the absence of sulfate anions on both ZFs as opposed to the
3 high concentration of 950 ng/m³ observed on the ground. These preliminary results are
4 consistent with nitrate being an important component of ATAL, as suggested by the model
5 results of Gu et al. (2016), with the additional presence of some mineral dust aerosol.

6

7 2. How does convection affect the ATAL ?

8 a. Convective influence on the measurements.

9

10 We assess the influence of convection on the BATAL measurements using a combined
11 approach with trajectory calculations and cloud top brightness temperature observations from
12 the HIMAWARI-8 geostationary satellite used as a proxy for deep convection. We used an
13 overshooting cloud and anvil detection algorithm described by Bedka and Khlopenkov
14 (2016) to find when and where measurements were likely affected by convection based on
15 backtrajectories initialized at the location of balloon measurements (Figure 11). Figure 12
16 (bottom) shows back-trajectories colored according to their respective altitudes and initialized
17 from the two Heavy balloon Flights (HF) from Hyderabad (08/08/15 and 08/13/15) between
18 14-18 km (Fig.11). We show only the trajectories influenced by deep convection during the
19 72 hours preceding the balloon measurements. The position of the convective systems are
20 shown with filled red circles. Air masses from the upper troposphere (~14km) tend to follow
21 trajectories within the inner core of the Asian Anticyclone, while those at higher altitudes
22 follow the edge. The flight on August 8th was likely influenced by regional convection
23 (within 10h of the flights) over the Bay of Bengal and along the Indian central and east shore.
24 Brightness temperatures indicate cloud tops reaching the upper troposphere but probably not
25 penetrating the tropopause. Aerosol concentration (Fig.11), backscatter and ozone
26 concentration (not shown) increases near 14-16 km may indicate the convective transport of

1 regional Indian pollution and its influence on these measurements. The peak in ozone (not
2 shown) could have been produced via photochemical production due to anthropogenic or
3 lightning-induced NO_x emissions.

4 The peak in aerosol concentration and water vapor (Fig.9C) near the cold point tropopause
5 observed on August 13th could have originated from earlier convection over the Bay of
6 Bengal, Thailand, Laos and South China where trajectories ~17 km appear to intersect deep
7 convective systems at these altitudes. However, identifying a specific convective system
8 influencing the measurements is complicated since convection frequently reaches the
9 tropopause during the ASM. It is easier to identify recent and regional MCSs affecting the
10 measurements due to the better accuracy of shorter trajectory calculations. During the 2016
11 BATAL campaign, we had a balloon flight in the vicinity of a deep convective system, which
12 will be discussed in the next section.

13
14 b. Overshoot of ice particles in the lower stratosphere.

15
16 We conducted a balloon flight on August, 12th 2016 during an active monsoon period
17 using the Boomerang controlled system (see section II). The time series of temperature,
18 altitude, ascent rate (colored) and COBALD scattering ratios at 455 nm and 940 nm are
19 shown in Fig 13. An abrupt decrease in the ascent rate from 6 m/s to 3 m/s near 14 km, 23
20 min after the launch, corresponds to the release of the secondary balloon. The valve of
21 Boomerang system was activated several times to reduce the ascent rate near 1-2 m/s and to
22 maintain a very slow ascent through the UTLS region. After crossing the cold point
23 tropopause (at 52 min) near 16.5 km (-80°C), the system reached the lower stratosphere and
24 sampled layers of elevated SR near 18.5-19 km. COBALD color index values above 10
25 associated with these stratospheric features indicate the likely presence of ice crystals. We

1 computed backtrajectories from the location of the balloon flight to determine if convection
2 could be associated with these layers. Figure 14a (left) shows a Himawari-8 10.4 micron
3 cloud top brightness temperature (BT) image across southeast Asia overlaid with colored
4 squares corresponding to the position and altitude of back-trajectory air parcels sampled by
5 the balloon ~36 hours later. Air parcels above 17.5 km intersected a Mesoscale Convective
6 System (MCS) over southeastern China at that time. A zoomed image of the MCS (Fig. 14b)
7 shows the presence of Overshooting cloud Tops (OT, black arrows) and Above-Anvil Cirrus
8 Plumes (AACP, white outlines). OTs were persistently generated by this MCS throughout its
9 lifetime, reaching 189 K BT, 4 K colder than the cold-point tropopause observed by the
10 nearby 12 Z sounding from Kunming, China. At the time of this image, AACPs, indicative
11 of injection of ice into the lower stratosphere (Setvak et al. 2010; Homeyer et al. 2017), were
12 being generated by OTs that intersected with the back-trajectories. The AACPs radiate at the
13 lower stratospheric temperature (~200 K, 18.5-19 km altitude according to the Kunming
14 sounding), which is 10+ K warmer than the OT BT. OT regions to the south had also
15 generated AACP earlier in the MCS lifetime. Though a 36-hour back trajectory has some
16 error, given that this MCS had repeatedly generated AACP throughout its north-south extent,
17 this MCS is a strong candidate to explain the presence of ice layers in the lower stratosphere
18 observed by the balloon. Other convective storm systems over India during the balloon
19 campaigns have also shown the signature of convection overshooting the cold point
20 tropopause and reaching the lower stratosphere, providing strong evidence that deep
21 convection during the Summer Asian Monsoon can influence the lower stratospheric
22 composition.

23

24

25

1 IV. Discussion.

2 3 a. ATAL and New Particle Formation

4
5 Balloon measurements made from the TIFR balloon facility, Hyderabad during BATAL
6 strongly suggest that the ATAL is composed primarily of small ($r < 0.25 \mu\text{m}$), liquid (mostly
7 volatile, ~80-95%) aerosol with or without solid cores, correlated with enhanced water vapor
8 and virtually no ozone. Moist layers observed near and above the cold point tropopause
9 suggest the influence of deep convection, which could also be responsible for transporting
10 aerosol and/or their gas-phase precursors. Up to 100 pptv of SO_2 were measured in the
11 Eastern part of the Asian Anticyclone during the Oxidation Mechanism Observation
12 campaign (H. Schlager, personal communication with D. Fairlie), suggesting that SO_2 , as a
13 precursor of sulfate aerosol, can survive convective storms and reach the upper troposphere.

14 We performed numerical simulations using the microphysical model M7 (Vignati et al.,
15 2004). The aerosol dynamic processes in M7 include nucleation, coagulation, and
16 condensation of sulfuric acid. Aerosol physical properties (size distributions and
17 concentrations) were calculated along back-trajectories initialized at the balloon locations and
18 using GEOS-5 meteorological fields. ~100 ppt of SO_2 was injected at the beginning and
19 along the trajectories when air parcels were influenced by deep convection (see section III.d).
20 Consistent with previous studies (Weigel et al., 2011, Crumeyrolle et al., 2010), sunlight, low
21 temperatures as well as low pressure are favorable to new particle formation. The fast vertical
22 transport, in deep convective storms, of gas-phase aerosol precursors from the surface up to
23 17 km is thus highly favorable to nucleation events. Within a few days (1.5 days on average),
24 aerosols grow by condensation and coagulation processes from a few nm to 100 nm. The
25 extinction coefficients, calculated using a Mie code with a refractive index of 1.521

1 (representative of ammonium sulfate ; Seinfeld and Pandis, 2006), ranges from $0.2 \cdot 10^{-3}$ to
2 $2.4 \cdot 10^{-3} \text{ km}^{-1}$ consistent with CALIOP observations. Moreover, SO_2 injected in the model
3 along the transport to simulate the influence of deep convection is found to condensate on
4 existing particles, enhancing the extinction coefficients by a factor of 1.5.

5

6 b. Cloud-aerosol relation in the UTLS.

7

8 Thin cirrus clouds have been observed very frequently near the cold point tropopause
9 during the BATAL campaigns. Coincident OPC/ COBALD measurements can be used to
10 investigate ATAL's interaction with clouds. Figure 11 shows the aerosol concentration
11 profiles for particles of radius between $0.075 \mu\text{m}$ and $0.15 \mu\text{m}$ measured during the two
12 heavy flights carried out from Hyderabad in 2015. Part of the profiles are colored in red when
13 the CI from COBALD is greater than 10 and indicate the presence of large ice particles also
14 observed through the larger channels of the Wyoming OPC (not shown). The concentration
15 of aerosol is very similar on both flights at altitudes above $\sim 18 \text{ km}$, 1 km above the cold point
16 tropopause (see arrows). We observe a sharp decrease of aerosol concentration from 10
17 part/cm^3 to $2 \text{ part}/\text{cm}^3$ between 18 and 20 km. We observe a strong variability within the two
18 profiles below 18 km with a factor of ~ 25 in aerosol concentration between the peaks near 17
19 km (08/13) and 15 km (08/08) compared to the minimum values near 16 km on both flights.
20 CN measurements during those two flights (not shown) were saturated throughout the
21 troposphere. However, these profiles converge (toward $\sim 20 \text{ part}/\text{cm}^3$) near 18-18.2 km like
22 those shown in Fig.10.

23 We also note that the aerosol minimum observed on 08/13 between 15-16 km is
24 associated with the presence of an ice cloud (red) layer as observed by COBALD. In
25 addition, the apparent drop in aerosol concentration near 17 km on 08/08 also coincides with

1 a thin cirrus cloud near the cold point tropopause. The presence of ice clouds associated with
2 reduction or minimum in aerosol concentration could be consistent with aerosol removal
3 processes such as in-cloud scavenging of aerosol droplets. In contrast, aerosol concentration
4 peaks suggest the presence of a source mechanism. Figure 9C shows an enhancement of
5 water vapor mixing ratio near 17-18 km coincident with the peak in aerosol concentration on
6 August 13th, also implying that the air masses at these levels were likely influenced by deep
7 convection. Thus, convectively influenced air masses appear to be a source of aerosols up to
8 1km above the cold point tropopause. Overall, these observations suggest that the aerosol
9 budget is balanced by source and removal mechanisms associated with convection up to 18
10 km, ~1km above the cold point tropopause in the monsoon region.

11

12 **Conclusion and perspective.**

13

14 We provide an overview of the balloon-borne activities from India and Saudi-Arabia
15 between 2014-2017 during the BATAL campaigns. With 68 balloon flights and payloads
16 dedicated to study UTLS aerosols, together with water vapor and ozone sensors, we show the
17 first set of advanced in-situ measurements of the ATAL with COBALD backscatter sonde,
18 OPC size distributions and offline chemical analysis. We found that the ATAL is comprised
19 of mostly small ($r < 0.25 \mu\text{m}$), liquid (~ 80-95%) aerosols with relatively low SR at 532nm
20 ($\text{SR} < 1.2$), consistent with CALIOP satellite observations. Chemical analysis of particles
21 collected near the tropopause indicates the dominant presence of nitrate aerosol with
22 concentration of about 100 ng/m^3 . Balloon and satellite observations consistently showed a
23 drop in aerosol concentration (CN, $r > 75 \text{ nm}$ (total), $r > 75 \text{ nm}$ (non-volatile aerosol)), and
24 backscatter near 18 km (~400-420 K), ~1km above the cold point tropopause, and 1-1.5 km
25 above the 380 K isentropic level. In addition, enhanced water vapor and ice particles have

1 been observed during the BATAL campaigns at and above the cold point tropopause. These
2 indicate that convection can potentially influence aerosol loadings well above the tropopause
3 level.

4 The first offline chemical analysis of the ATAL reveals interesting but puzzling
5 results. The presence of nitrate aerosol can be possibly explained by the gas-to-aerosol
6 conversion of HNO_3 from NO_x produced through lightning or transported by convection
7 from the boundary Layer (Gu et al., 2016). However, the absence of sulfate aerosol seems to
8 be contradictory with the expectation of increasing influence of sulfur emissions in Asia over
9 the past few decades on aerosol trends in the UTLS (Vernier et al., 2015).

10 Additional observations are needed to address these puzzling questions. NO_x/NO_y
11 measurements would help constrain the role of gas-to-aerosol conversion in the formation of
12 nitrate aerosol. Additional pollution tracers, such as CO, would help to determine the relative
13 importance of in situ lightning production of NO_x versus convective transport from polluted
14 regions to the abundance of nitrate aerosol. In addition, online aerosol mass spectroscopy
15 would help understanding whether volatile aerosols (e.g. NH_4), which would disappear
16 during offline analysis, could be present in the ATAL. A suite of aerosol and ice
17 measurements would contribute to an improved understanding of aerosol-cloud
18 interactions in the UTLS region. In order to study the impact of the ATAL on heterogeneous
19 ozone chemistry, ClO and ClONO₂ would also need to be measured. The BATAL project has
20 been approved to continue for another 3-4 years, and NASA and ISRO aim to augment their
21 level of collaboration on this program. Additional balloon payloads will
22 be considered to help address the remaining science questions regarding the composition of
23 the ATAL and its interaction with convection and cirrus clouds. Additionally, the results of
24 the BATAL campaigns will be used to formulate a future NASA-ISRO airborne campaign
25 with NASA high altitude aircraft.

1 **Acknowledgement**

2
3
4
5
6
7
8
9
10
11
12
13
14
15
16
17
18
19
20
21
22
23
24
25
26

We thank Drs. J. Kaye and K. Jucks at NASA HQ for supporting the BATAL campaigns since 2014 through the UARP program. We acknowledge technicians and engineers from NARL, TIFR, BHU and KAUST for their help during BATAL. We also thank the Indian Meteorological Department for providing Doppler weather radar images and MOSDAC for providing INSAT-3D satellite images. We acknowledge Timothy Marvel for his help to make Fig.1. We also thank Jacquelyn Charity-Hodnett and Kishore Kumar for their logistical supports.

LABEX VOLTAIRE "Étude des géofluides et des VOLatils-Terre, Atmosphère et Interfaces-Ressources et Environnement" (VOLTAIRE) (ANR-10-LABX-100-01) managed by the University of Orléans.

The GEOS-5 data used in this study have been provided by the Global Modeling and Assimilation Office (GMAO) at NASA Goddard Space Flight Center through the online data portal in the NASA Center for Climate Simulation.

1 **References**

2
3
4
5
6
7
8
9
10
11
12
13
14
15
16
17
18
19
20
21
22
23
24
25
26
27

Bedka, K.M. and K. Khlopenkov, 2016: A Probabilistic Multispectral Pattern Recognition Method for Detection of Overshooting Cloud Tops Using Passive Satellite Imager Observations. *J. Appl. Meteor. Climatol.*, **55**, 1983–2005, doi: 10.1175/JAMC-D-15-0249.1.

Campbell, P., and T. Deshler (2014), Condensation nuclei measurements in the midlatitude (1982-2012) and Antarctic (1986-2010) stratosphere between 20 and 35 km, *J. Geophys. Res. Atmos.*, 119, doi:10.1002/2013JD019710.

Deshler, T., M. E. Hervig, D. J. Hofmann, J. M. Rosen, and J. B. Liley, Thirty years of in situ stratospheric aerosol size distribution measurements from Laramie, Wyoming (41N), using balloon-borne instruments, *J. Geophys. Res.*, *108(D5)*, 4167, doi:10.1029/2002JD002514, 2003.

Crumeyrolle, S., Manninen, H.E., Sellegri, K., Roberts, G., Gomes, L., Kulmala, M., Weigel, R., Laj, P., Schwarzenboeck, A., 2010. New particle formation events measured on board the ATR-42 aircraft during the EUCAARI campaign. *Atmos. Chem. Phys.* 10, 6721–6735. doi:10.5194/acp-10-6721-2010

Garny, H. and Randel, W. J.: Transport pathways from the Asian monsoon anticyclone to the stratosphere, *Atmos. Chem. Phys.*, 16, 2703-2718, doi:10.5194/acp-16-2703-2016, 2016.

Gu, Y., H. Liao , and J. Bian, Summertime nitrate aerosol in the upper troposphere and lower stratosphere over the Tibetan Plateau and the South Asian summer monsoon region, *Atmos. Chem. Phys.*, 16, 6641–6663, 2016.

Kim, Y.-S., Shibata, T., Iwasaka, Y., Shi, G., Zhou, X., Tamura, K., Ohashi, T., (2003), Enhancements of aerosols near the cold tropopause in summer over Tibetan Plateau: Lidar and balloon borne measurements in 1999 at Lhasa, Tibet, China. *Proc. SPIE* 4893, 496–503.

1
2 Komhyr, W. D., R. A. Barnes, G. B. Brothers, J. A. Lathrop, and D. P. Opperman,
3 Electrochemical concentration cell ozonesonde performance evaluation during STOIC
4 1989, *J. Geophys. Res.*, 100, 9231 – 9244, 1995.

5 Kremser, S., et al. (2016), Stratospheric aerosol—Observations, processes, and impact on
6 climate, *Rev. Geophys.*, 54, 278–335, doi:[10.1002/2015RG000511](https://doi.org/10.1002/2015RG000511).

7 Krotkov, N. A., McLinden, C. A., Li, C., Lamsal, L. N., Celarier, E. A., Marchenko, S. V.,
8 Swartz, W. H., Bucsela, E. J., Joiner, J., Duncan, B. N., Boersma, K. F., Veefkind, J.
9 P., Levelt, P. F., Fioletov, V. E., Dickerson, R. R., He, H., Lu, Z., and Streets, D. G.:
10 Aura OMI observations of regional SO₂ and NO₂ pollution changes from 2005 to
11 2015, *Atmos. Chem. Phys.*, 16, 4605–4629, doi:[10.5194/acp-16-4605-2016](https://doi.org/10.5194/acp-16-4605-2016), 2016.

12 Lawrence, M. G. and Lelieveld, J. (2010), Atmospheric pollutant outflow from southern Asia:
13 a review, *Atmos. Chem. Phys.*, 10, 11017–11096, doi:[10.5194/acp-10-11017-2010](https://doi.org/10.5194/acp-10-11017-2010).

14 Lau, W.K.M., Kim, K.M., Shi, J.J. et al. *Clim Dyn* (2016). doi:[10.1007/s00382-016-3430-y](https://doi.org/10.1007/s00382-016-3430-y)

15 Lurton, T., Renard, J.-B., Vignelles, D., Jeannot, M., Akiki, R., Mineau, J.-L., Tonnelier, T.,
16 2014. Light scattering at small angles by atmospheric irregular particles: modelling
17 and laboratory measurements. *Atmospheric Meas. Tech.* 7, 931–939.
18 doi:[10.5194/amt-7-931-2014](https://doi.org/10.5194/amt-7-931-2014).

19 Molod, A., L. Takacs, M. Suarez, J. Bacmeister, I. Song, and A. Eichmann, *The GEOS-5*
20 *Atmospheric General Circulation Model: Mean Climate and Development from*
21 *MERRA to Fortuna*, Technical Report Series on Global Modeling and Data
22 Assimilation, 28, Ed: Max J. Suarez, NASA GMAO, Goddard Space Flight Center,
23 Greenbelt, MD, April 2012.

24 Pandit, A. K., Gadhavi, H. S., Venkat Ratnam, M., Raghunath, K., Rao, S. V. B., and
25 Jayaraman, A.: Long-term trend analysis and climatology of tropical cirrus clouds

1 using 16 years of lidar data set over Southern India, *Atmos. Chem. Phys.*, 15, 13833-
2 13848, doi:10.5194/acp-15-13833-2015, 2015.

3 Park, R. J., D. J. Jacob, B. D. Field, R. M. Yantosca, and M. Chin, 2004, Natural and
4 transboundary pollution influences on sulfate-nitrate-ammonium aerosols in the United
5 States: Implications for policy, *J. Geophys. Res.*, 109, D15204,
6 doi:10.1029/2003JD004473.

7 Park, M., W.J. Randel, A. Gettelman, S. Massie and J. Jiang, Transport above the Asian
8 summer monsoon anticyclone inferred from Aura MLS tracers (2007), *J. Geophys.*
9 *Res.*, 112, D16309, doi:10.1029/2006JD008294.

10 Randel, W. J., M. Park, L. Emmons, D. Kinnison, P. Bernath, K. A. Walker, C. Boone, H.
11 Pumphrey (2010), Asian Monsoon Transport of Pollution to the Stratosphere, *Science*,
12 328, 611 – 613, doi: 10.1126/science.1182274.

13 Randel, W.J., and M. Park (2006), Deep convective influence on the Asian summer monsoon
14 anticyclone and associated tracer variability observed with AIRS, *J. Geophys. Res.*,
15 111, D12314, doi:10.1029/2005JD006490.

16 Renard, J.-B., Dulac, F., Berthet, G., Lurton, T., Vignelles, D., Jégou, F., Tonnelier, T.,
17 Jeannot, M., Couté, B., Akiki, R., Verdier, N., Mallet, M., Gensdarmes, F.,
18 Charpentier, P., Mesmin, S., Duverger, V., Dupont, J.-C., Elias, T., Crenn, V., Sciare,
19 J., Zieger, P., Salter, M., Roberts, T., Giacomoni, J., Gobbi, M., Hamonou, E.,
20 Olafsson, H., Dagsson-Waldhauserova, P., Camy-Peyret, C., Mazel, C., Décamps, T.,
21 Piringer, M., Surcin, J., Daugeron, D., 2016. LOAC: a small aerosol optical
22 counter/sizer for ground-based and balloon measurements of the size distribution and
23 nature of atmospheric particles – Part 1: Principle of measurements and instrument
24 evaluation. *Atmospheric Meas. Tech.* 9, 1721–1742. doi:10.5194/amt-9-1721-2016.

1 Rienecker, M.M., M.J. Suarez, R. Todling, J. Bacmeister, L. Takacs, H.-C. Liu, W. Gu, M.
2 Sienkiewicz, R.D. Koster, R. Gelaro, I. Stajner, and E. Nielsen, 2008: *The GEOS-5*
3 *Data Assimilation System - Documentation of Versions 5.0.1, 5.1.0, and*
4 *5.2.0. Technical Report Series on Global Modeling and Data Assimilation*
5 *104606*, v27.

6 Setvak et al., 2010, D.T. Lindsey, P. Novk, P.K. Wang, M. Radov, J. Kerkmann, L. Grasso,
7 S.H. Su, R.M. Rabin, J. Stastka, Satellite-observed cold-ring-shaped features atop
8 deep convective clouds, *Atmos. Res.*, 97 (2010), pp. 80–96

9 Solomon, S., et al. (2016), Monsoon circulations and tropical heterogeneous chlorine
10 chemistry in the stratosphere, *Geophys. Res. Lett.*, 43, 12,624–12,633,
11 doi:[10.1002/2016GL071778](https://doi.org/10.1002/2016GL071778).

12 Seinfeld J.H. and S.N. Pandis : *Atmospheric Chemistry and Physics: From Air Pollution to*
13 *Climate Change*, 3rd Edition - Wiley

14 Thomason, L. W. and Vernier, J.-P. (2013), Improved SAGE II cloud/aerosol categorization
15 and observations of the Asian tropopause aerosol layer: 1989–2005, *Atmos. Chem. Phys.*,
16 13, 4605-4616, doi:[10.5194/acp-13-4605-2013](https://doi.org/10.5194/acp-13-4605-2013).

17 Tobo, Y., et al, (2007), Balloon-borne observations of high aerosol concentrations near the
18 summertime tropopause over the Tibetan Plateau, *Atmos. Res.*, 84, 233-241.

19

20 Vernier, J.-P., L. W. Thomason, and J. Kar (2011a) CALIPSO detection of an Asian
21 tropopause aerosol layer , *Geophys. Res. Lett.*, Vol. 38, L07804,
22 doi:[10.1029/2010GL046614](https://doi.org/10.1029/2010GL046614).

23 Vernier, J. -P. , Fairlie, T. D., Natarajan, M., Wienhold, F. G., Bian, J., Martinsson, B.
24 G., Crumeyrolle, S., Thomason, L. W. and Bedka, K. M. (2015), Increase in upper
25 tropospheric and lower stratospheric aerosol levels and its potential connection with

1 Asian pollution. *J. Geophys. Res. Atmos.*, 120: 1608–1619.
2 doi: [10.1002/2014JD022372](https://doi.org/10.1002/2014JD022372).

3 Vernier, J.-P., J. P. Pommereau, A. Garnier, J. Pelon, N. Larsen, J. Nielsen, T. Christensen, F.
4 Cairo, L. W. Thomason, T. Leblanc, and I. S. McDermid (2009), Tropical stratospheric
5 aerosol layer from CALIPSO lidar observations, *J. Geophys. Res.*, 114, D00H10,
6 doi:10.1029/2009JD011946.

7 Vignati, E., J. Wilson, and P. Stier (2004), M7: An efficient size-resolved aerosol
8 microphysics module for large-scale aerosol transport models, *J. Geophys. Res.*, 109,
9 D22202, doi:10.1029/2003JD004485.

10 Bärbel Vogel, Gebhard Günther, Rolf Müller, Jens-Uwe Grooß, Armin Afchine, Heiko
11 Bozem, Peter Hoor, Martina Krämer, Stefan Müller, Martin Riese, Christian Rolf, Nicole
12 Spelten, Gabriele P. Stiller, Jörn Ungermann, and Andreas Zahn, Long-range transport
13 pathways of tropospheric source gases originating in Asia into the northern lower
14 stratosphere during the Asian monsoon season 2012, *Atmos. Chem. Phys. Discuss.*,
15 doi:10.5194/acp-2016-463, 2016.

16 Vömel, H., D. E. David, and K. Smith (2007), Accuracy of tropospheric and stratospheric
17 water vapor measurements by the cryogenic frost point hygrometer: Instrumental
18 details and observations, *J. Geophys. Res.*, 112, D08305, doi:10.1029/2006JD007224.

19 Weigel, R., Borrmann, S., Kazil, J., Minikin, A., Stohl, A., Wilson, J.C., Reeves, J.M.,
20 Kunkel, D., de Reus, M., Frey, W., Lovejoy, E.R., Volk, C.M., Viciani, S., D'Amato,
21 F., Schiller, C., Peter, T., Schlager, H., Cairo, F., Law, K.S., Shur, G.N., Belyaev,
22 G.V., Curtius, J., 2011. In situ observations of new particle formation in the tropical
23 upper troposphere: the role of clouds and the nucleation mechanism. *Atmos. Chem.*
24 *Phys.* 11, 9983–10010. doi:10.5194/acp-11-9983-2011.

1 Yu Pengfei, Karen H. Rosenlof, Shang Liu, Hagen Telg, Troy D. Thornberry, Andrew W.
2 Rollins, Robert W. Portmann, Zhixuan Bai, Eric A. Ray, Yunjun Duan, Laura L. Pan,
3 Owen B. Toon, Jianchun Bian, and Ru-Shan Gao. Efficient transport of tropospheric
4 aerosol into the stratosphere via the Asian summer monsoon anticyclone. PNAS 2017
5 114: 6972-6977.

6
7
8
9
10
11
12
13
14
15
16
17
18
19
20
21
22
23
24
25

1 **Figure captions.**

2 Figure 1. (1) *Deep convection from the Asian Summer Monsoon transports air masses from*
3 *the boundary layer to the Upper Troposphere and Lower Stratosphere (UTLS). An overpass*
4 *of the CALIPSO lidar on August 12th 2017 at 19h30 UTC shows the vertical extension of*
5 *convection through backscatter measurements. (2) The monsoonal outflow is transported*
6 *through tropical easterlies prevailing in the UTLS along the southern branch of the Asian*
7 *Anticyclone. (3) Air in the tropical upper troposphere along the southern edge of the Asian*
8 *Anticyclone can be uplifted into the lower stratosphere via diabatic ascent. The Asian*
9 *Tropopause Aerosol Layer (ATAL) is a pool of aerosols filling the Asian Anticyclone shown*
10 *as light yellowish color.*

11

12 Figure 2. *Balloon trajectories from Gadanki [13.46°N, 79.17°E], Hyderabad [17.47°N,*
13 *78.58°E], Varanasi [25.27°N, 82.99°E] and Thuwal [22.32°N, 39.10°E] during the BATAL*
14 *campaigns between 2014 and 2017. The ascending and descending balloon profiles are*
15 *shown in orange and magenta, respectively.*

16

17 Figure 3. *Ballooning during BATAL. Preparation of: (1) Heavy balloon Flights (HF) from*
18 *Hyderabad using plastic balloons. (2) Regular Medium and Light-weight balloon Flights*
19 *(MF/LF) with latex balloons. (3) Zero-pressure balloon Flight (ZF) using plastic balloon. (4)*
20 *Controlled flight using the Boomerang system attached to the neck of the balloon.*

21

22 Figure 4. *Sketch of the Static Launch Method used during the zero-pressure flights at the*
23 *TIFR balloon facility, Hyderabad. (1) The ballast module holds up to 25 kg of fine metallic*
24 *balls which are released per packet of 1 kg. (2) The science payloads include an aerosol*
25 *impactor, a COBALD backscatter sonde, an ozonesonde, and an meteorological sondes. (3)*

1 *The communication package is used to release ballast on commands, terminate the flight*
2 *through the pyrocutter and send GPS data through radio-communication. (4)The plastic*
3 *balloon is filled with hydrogen and has a volume of 300 m³.*

4
5 *Figure 5. Time evolution of the GPS altitude four zero-pressure balloon flights on August 10th*
6 *2015, August 8th, 15th and 21st 2017.*

7
8 *Figure 6. Concentrations of carbon monoxide (CO), sulfate, nitrate, and black carbon (BC)*
9 *at 100 hPa on 21 UTC, August 3, 2017, as predicted by the NASA GEOS-5 Forward*
10 *Processing (FP) forecasting system on 00 UTC, July 30, 2017. Arrows denote winds. White*
11 *dots along the white line (G and H) indicate two balloon sounding locations, Gadanki*
12 *and Hyderabad, respectively.*

13
14 *Figure 7. Map of Scattering Ratio (SR) at 532 nm after averaging the CALIPSO cloud-*
15 *cleared data between 16-18 km in Jul-August 2015. Corresponding cross-sections from*
16 *averaged data between 15 °N-45 °N (bottom) and 5 °E-105 °E (right) depict the 3-D extension*
17 *of the ATAL. The white lines show isopleths of potential temperature (K). The locations of the*
18 *balloon launches during the BATAL deployments are shown by red diamonds on the map and*
19 *red lines on the cross-section. [1. Gadanki, 2. Hyderabad, 3. Thuwal, 4. Varanasi].*

20
21 *Figure 8. SR profiles (black stars) at 532 nm derived from the COBALD balloon flights in*
22 *Thuwal between 5-12 August 2015 (left) and Gadanki-Hyderabad between 17 July and 13*
23 *August 2015 (right). Averaged COBALD profiles (black line) and CALIPSO profiles (red*
24 *line) within +/-5 ° latitude and +/- 30 ° longitude are shown. Radiosonde individual (blue*
25 *stars) and averaged (blue line) temperature profiles are also shown.*

1
2
3
4
5
6
7
8
9
10
11
12
13
14
15
16
17
18
19
20
21
22
23
24
25

Figure 9. Heavy balloon flight ascent profile of data collected on August 13th, 2015 from Hyderabad. (A) Particle Number Concentration (PNC) profiles from unheated Optical Particle Counter (OPC) for radius: $r > 0.075$, > 0.15 , > 0.25 , > 0.5 μm and Condensation Nuclei (CN) profile. (B) PNC profiles for $r > 0.075$ μm from heated (180°C) and unheated OPCs. (C) Temperature, ozone partial pressure and water vapor mixing ratio profiles. (D) SR at 940 nm and Color Index ($CI = (SR_{940} - 1) / (SR_{455} - 1)$) profiles from COBALD.

Figure 10. Cations and anions concentration obtained from Ion Chromatography analysis to derive the composition of aerosols collected on board ZF2, ZF3 and on the ground (GND) during the 2017 BATAL campaign.

Figure 11. Aerosol concentration profiles for particles within $0.075 \mu\text{m} < r < 0.15 \mu\text{m}$ from the 2015 heavy balloon flights on 08/08 and 08/13 in Hyderabad. Part of the profiles where COBALD detected ice clouds based upon the Color Index(CI) is colored in Red. We note that the CI profile below 15 km on 08/08 was too noisy to apply the CI criteria.

Figure 12. Back trajectories initialized from the balloon flights on 08/13/2015 (top) and 08/08/2015 (bottom) from Hyderabad. Red dots along these trajectories correspond to the presence of convection reaching the upper troposphere as seen by the HIMAWARI-8 geostationary satellite.

Figure 13. (Top) Altitude, temperature, scattering ratios at 455nm and 940 nm and Color Index (CI) time series along the Boomerang flight launched from Varanasi on 08/12/2016.

1 *Figure 14. (a) A Himawari-8 10.4 micron brightness temperature image at 1400 UTC on 11*
2 *August 2016 over Southeast Asia. Back-trajectory air parcels at the time of the image,*
3 *initialized from balloon flight position launched from Varanasi (India) 32 hours after,*
4 *colored by their altitude, are overlaid. (b) A zoomed image at 1410 UTC over the region*
5 *outlined by the red box in panel (a), contrast enhanced to more clearly show overshooting*
6 *cloud tops (black arrows) and above-anvil cirrus plumes (white outline), embedded within*
7 *the anvil of this mesoscale convective system. The locations of back-trajectory parcels above*
8 *17.5 km from 11-17 UTC are overlaid with white circles, illustrating the uncertainty in parcel*
9 *position at the time of the satellite image.*

10
11
12
13
14
15
16
17
18
19
20
21
22
23
24
25

Flight type	Approx. Payload weight	Balloon type	Measurements
Heavy Flight (HF)	>30 kg	H ₂ filled 3000 m ³ Polyethylene	<i>Particle size distribution, volatility, ozone, water vapour, particle backscatter and meteorological parameters</i>
Zero-pressure Flight (ZF)	> 10 kg	H ₂ filled 300 m ³ Polyethylene	<i>Extended aerosol measurements near tropopause</i>
Medium Flight (MF)	1.3kg <MF<10 kg	H ₂ filled 2000g/ 3000g Latex	<i>Combined Particle backscatter/ozone/water vapour/particle size distribution</i>
Light Flight (LF)	<1.3 kg	H ₂ filled 1200g Latex	<i>Particle backscatter/ meteorological parameters</i>
Boomerang Flight (BF)	<10 kg	H ₂ /He filled, tandem balloons, 2000g / 1200g	<i>Particle sampling using impactor with controlled ascent rate</i>

1 *Table 1. Balloon flight types during BATAL.*

2

3

4

5

6

7

8

9

Campaign	Location	Flights	Payloads
BATAL 2014 August	Gadanki [13.46°N, 79.17°E]	6 LF	Imet, COBALD, Lan OPC
		1 MF	
BATAL 2015 July-August	Gadanki [13.46°N, 79.17°E]	4 LF	Imet, COBALD, Lan OPC, CFH, O ₃
		2 MF	
BATAL 2015 July-August	Hyderabad [17.47°N, 78.58°E]	1 LF	Imet, COBALD, CFH, O ₃ , Lan OPC, Wyo OPC, Wyo OPCH, Wyo CN
		6 MF	
		1 ZF	
		2 HF	
BATAL 2015 July-August	Varanasi [25.27°N, 82.99°E]	1 LF	Imet, COBALD, CFH, O ₃ , Lan OPC, LOAC, Impactor
		5 MF	
		1 BF	
BATAL 2015 July-August	Thuwal [22.32°N, 39.10°E]	6 LF	Imet, COBALD
BATAL 2016	Gadanki [13.46°N, 79.17°E]	1 LF	Imet, COBALD, CFH, O ₃
		4 MF	
BATAL 2016 July-August	Varanasi [25.27°N, 82.99°E]	4 MF	Imet, COBALD, O ₃ , Lan OPC, Impactor
		2 BF	
BATAL 2016 July-August	Thuwal [22.32°N, 39.10°E]	5 LF	Imet, COBALD
BATAL 2017 July-August	Gadanki [13.46°N, 79.17°E]	1 LF	Imet, COBALD, O ₃ , CFH, Lan OPC, Meisei CPS
		5 MF	
BATAL 2017 July-August	Hyderabad [17.47°N, 78.58°E]	4 MF	Imet, COBALD, O ₃ , CFH, Lan OPC, Boulder OPC, MCPC, Impactor
		3 ZF	
		2 HF	

1

2 *Table 2. BATAL flights summary. To differentiate the OPCs, we use the syntax: Lan for*

3 *Langley, Wyo for Wyoming and LOAC)*

4

5

6

7

8

9

10

BATAL payloads	Lab/Company	Measured parameters	Measurement technique
Imet Radiosonde	Imet	Temp, Press, RH, Wind speed/direction	Piezoresistive, thermistor, capacitive
Ozonesonde	Droplet meas. tech., USA	Ozone concentration	Electrochemical
Cryogenic Froist Point Hygro	Droplet measurements	Water vapor concentration (UTLS)	child mirror principle
COBALD backscatter sonde	ETH, Swissserland	Scattering Ratio at 455 and 940 nm	Light scattering with diodes
Lan Optical Particle Counter	NASA Langley, USA	Aerosol conc. (8 ch/0.15-5 μm)	Laser counting
Wyo Optical Particle Counter 1	University of Wyoming, USA	Aerosol conc. (8 ch /0.075-15 μm)	Laser counting
Wyo Heated inlet/ OPCH	University of Wyoming, USA	Aerosol conc (8 ch /0.075-15 μm)	Laser counting
Wyo CN Counter	University of Wyoming, USA	Aerosol concentration (r>few nm)	Saturation chamber/Laser counting
LOAC	LPC2E France	Aerosol concentration (19 ch /0.1-50 μm)	Laser counting
Balloon-borne Aerosol Impactor	Calif. meas./ NASA Langley, USA	chemical composition	Aerodynamical impaction
Boulder Counter	LightHouse/NASA Langley, USA	Ice measurements (6 ch /5 μm -100 μm)	Laser counting
Mixing Cloud Particle Counter	Bretchel/ NASA Langley, USA	Aerosol concentration (r>few nm)	Saturation chamber/Laser counting

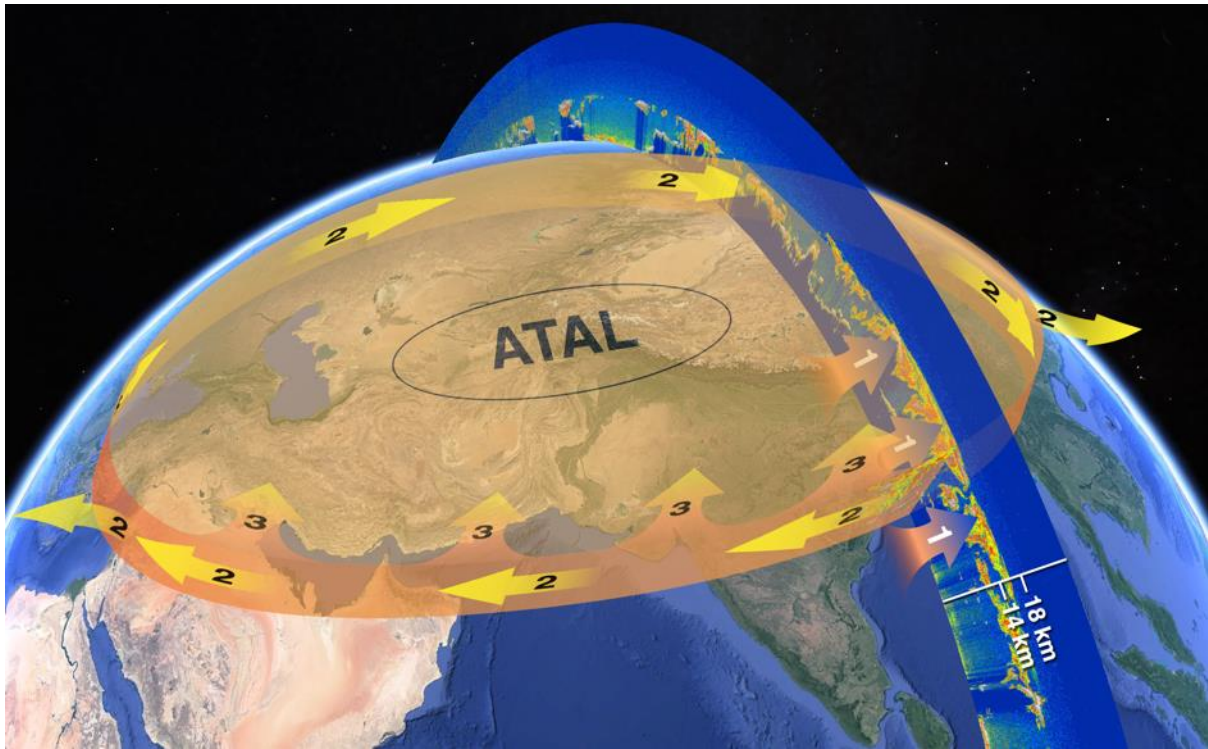
1
2 *Table 3. Information on the payloads flown during the BATAL campaigns. The aerosol size is*
3 *expressed in radius.*

4
5
6
7
8
9
10
11
12
13
14
15
16
17
18
19
20

Location	Instruments	Measured parameters	Spatial and temporal resolutions and mode of operation
Gadanki/India	Indian MST Radar	Turbulence parameters, 3-D wind profiles (Zonal, Meridional and Vertical)	150 m, 1 minute, continuous throughout the campaign
Gadanki/India	Mie and Rayleigh Lidar	Cirrus properties, Aerosols and temperature profiles	300 m, 4 minutes, continuous throughout the campaign
Gadanki/India	Lidar for Atmospheric measurement and Probing (LAMP)	Attenuated backscatter signal, Aerosol extinction profile, Boundary layer height, Cloud base height, Optical depth for optically thin clouds	30 m, 1 minute, continuous throughout the campaign
Gadanki/India	Surface measurements	Temperature, Relative humidity, wind speed and direction, rainfall	Surface, 1 minute, continuous throughout the campaign
Thuwal/Saudi-Arabia	Micro pulse lidar	Attenuated backscatter and depolarization at 532 nm	
Thuwal/Saudi-Arabia	AERONET/ Sunphotometer	Radiance and derived aerosol distribution.	

1 Table 4. Ground-based measurement support during BATAL.

2



1

2 *Figure 1. (1) Deep convection from the Asian Summer Monsoon transports air masses from*
 3 *the boundary layer to the Upper Troposphere and Lower Stratosphere (UTLS). An overpass*
 4 *of the CALIPSO lidar on August 12th 2017 at 19h30 UTC shows the vertical extension of*
 5 *convection through backscatter measurements. (2) The monsoonal outflow is transported*
 6 *through tropical easterlies prevailing in the UTLS along the southern branch of the Asian*
 7 *Anticyclone. (3) Air in the tropical upper troposphere along the southern edge of the Asian*
 8 *Anticyclone can be uplifted into the lower stratosphere via diabatic ascent. The Asian*
 9 *Tropopause Aerosol Layer (ATAL) is a pool of aerosols filling the Asian Anticyclone shown*
 10 *as light yellowish color.*

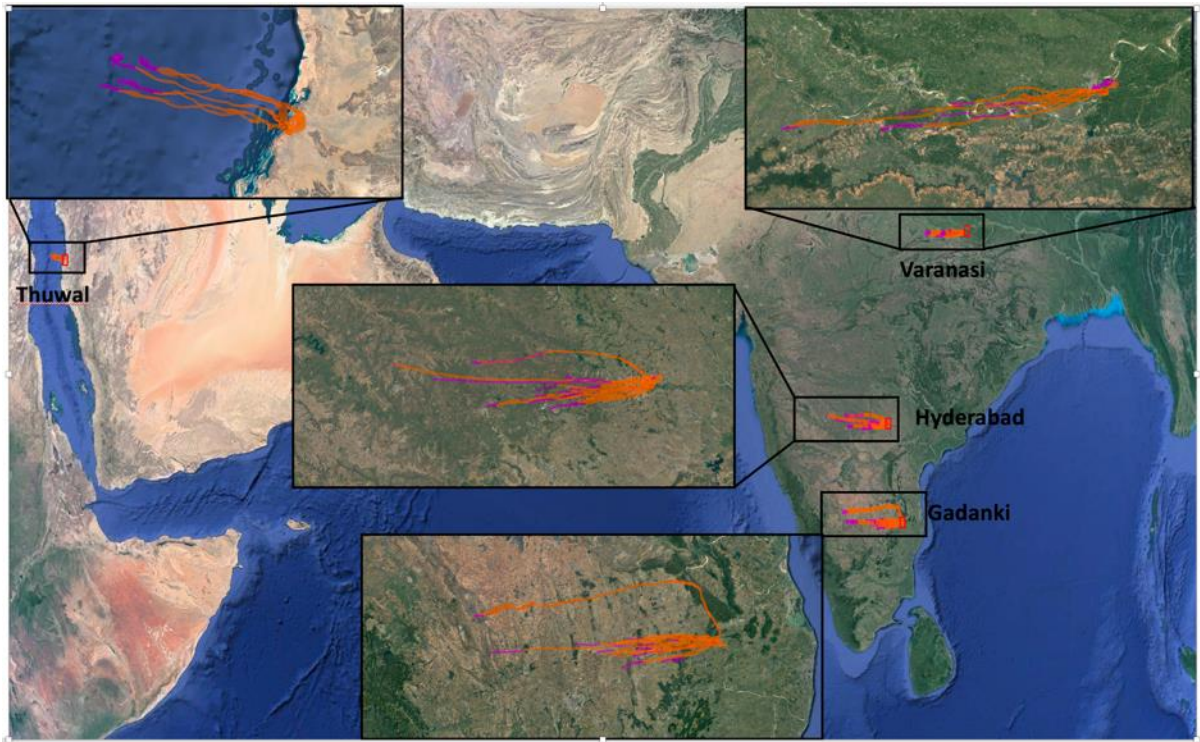
11

12

13

14

15



1
 2 *Figure 2. Balloon trajectories from Gadanki [13.46°N, 79.17°E], Hyderabad [17.47°N,*
 3 *78.58°E], Varanasi [25.27°N, 82.99°E] and Thuwal [22.32°N, 39.10°E] during the BATAL*
 4 *campaigns between 2014 and 2017. The ascending and descending balloon profiles are*
 5 *shown in orange and magenta, respectively.*

6
 7
 8
 9
 10

1. Heavy plastic balloon flight



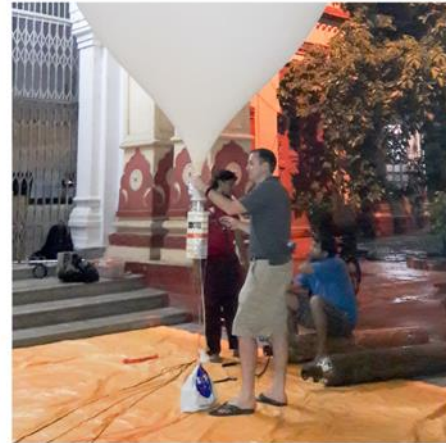
2. Regular latex balloon flights



3. Zero pressure flight



4. Boomerang flight



1

2 *Figure 3. Ballooning during BATAL. Preparation of: (1) Heavy balloon Flights (HF) from*
3 *Hyderabad using plastic balloons. (2) Regular Medium and Light-weight balloon Flights*
4 *(MF/LF) with latex balloons. (3) Zero-pressure balloon Flight (ZF) using plastic balloon. (4)*
5 *Controlled flight using the Boomerang system attached to the neck of the balloon.*

6

7

8

9

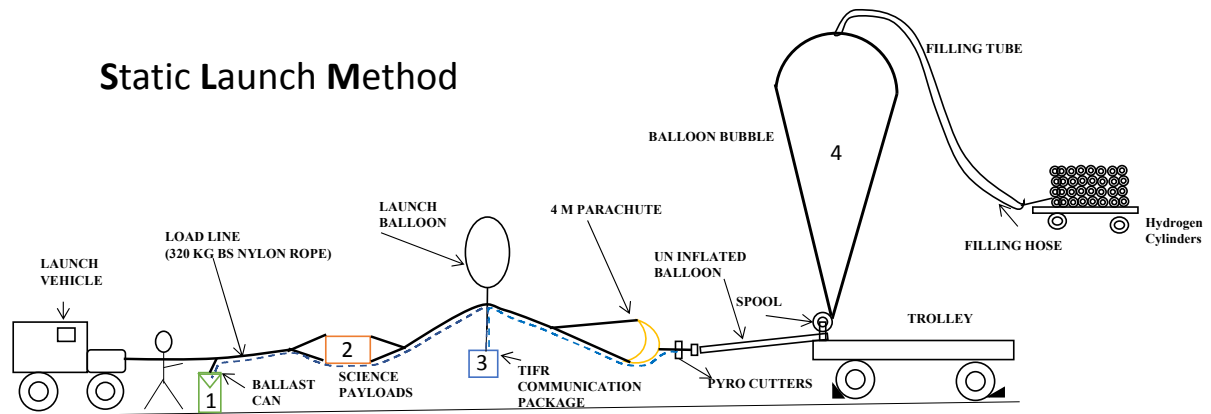
10

11

12

13

Static Launch Method



1

2 *Figure 4. Sketch of the Static Launch Method used during the zero-pressure flights at the*

3 *TIFR balloon facility, Hyderabad. (1)The ballast module holds up to 25 kg of fine metallic*

4 *balls which are released per packet of 1 kg. (2)The science payloads include an aerosol*

5 *impactor, a COBALD backscatter sonde, an ozonesonde, and an meteorological sondes. (3)*

6 *The communication package is used to release ballast on commands, terminate the flight*

7 *through the pyrocutter and send GPS data through radio-communication. (4)The plastic*

8 *balloon is filled with hydrogen and has a volume of 300 m³.*

9

10

11

12

13

14

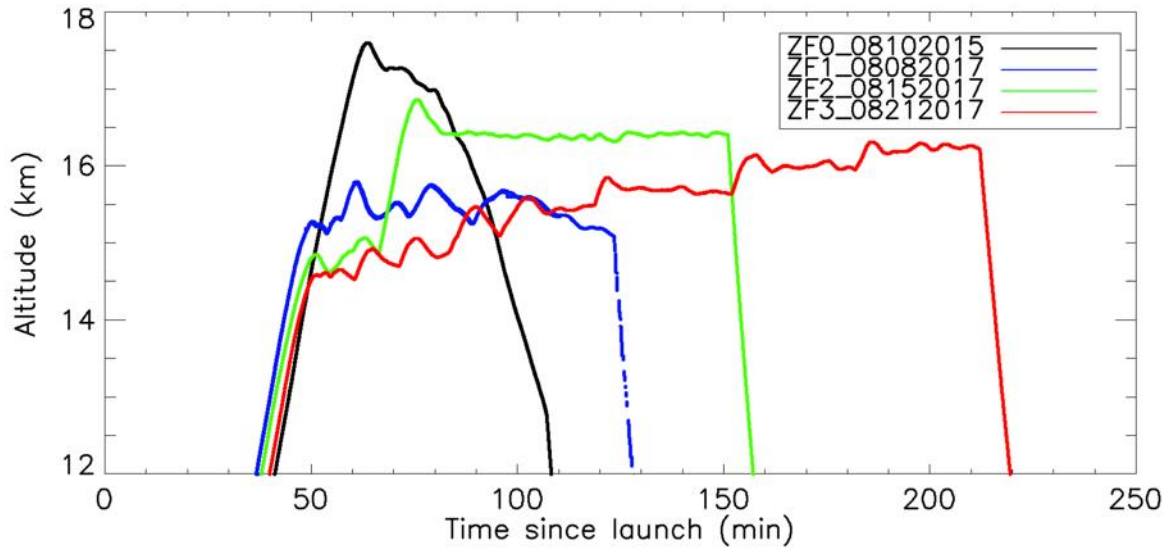
15

16

17

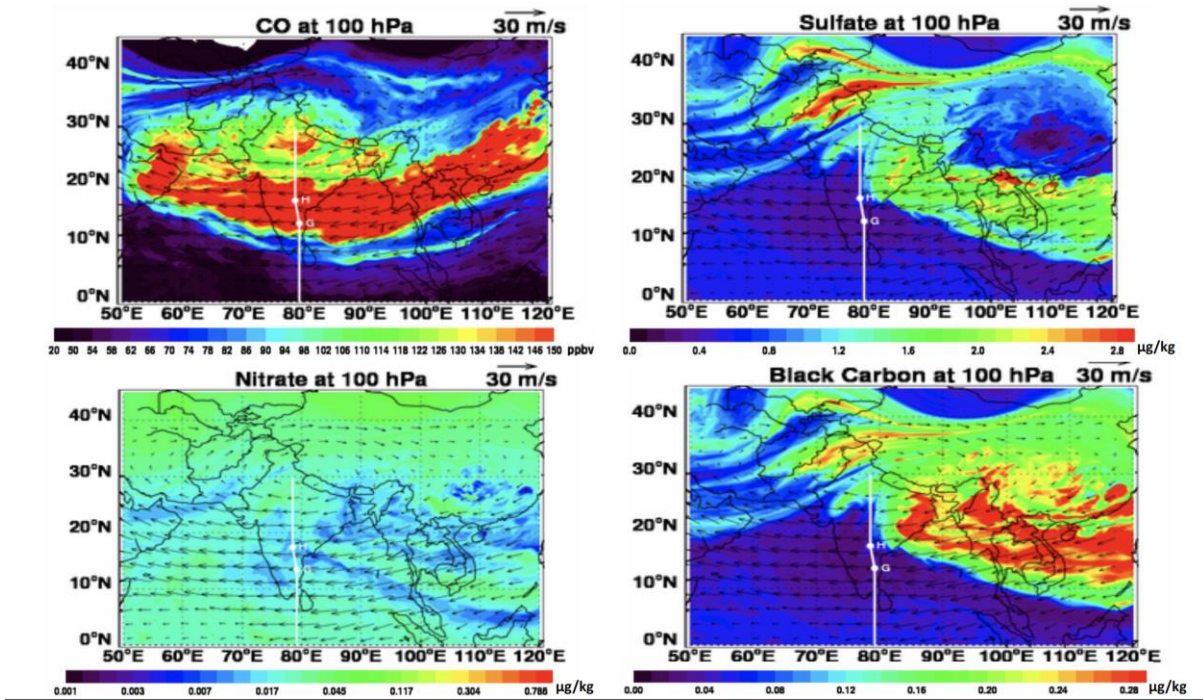
18

19



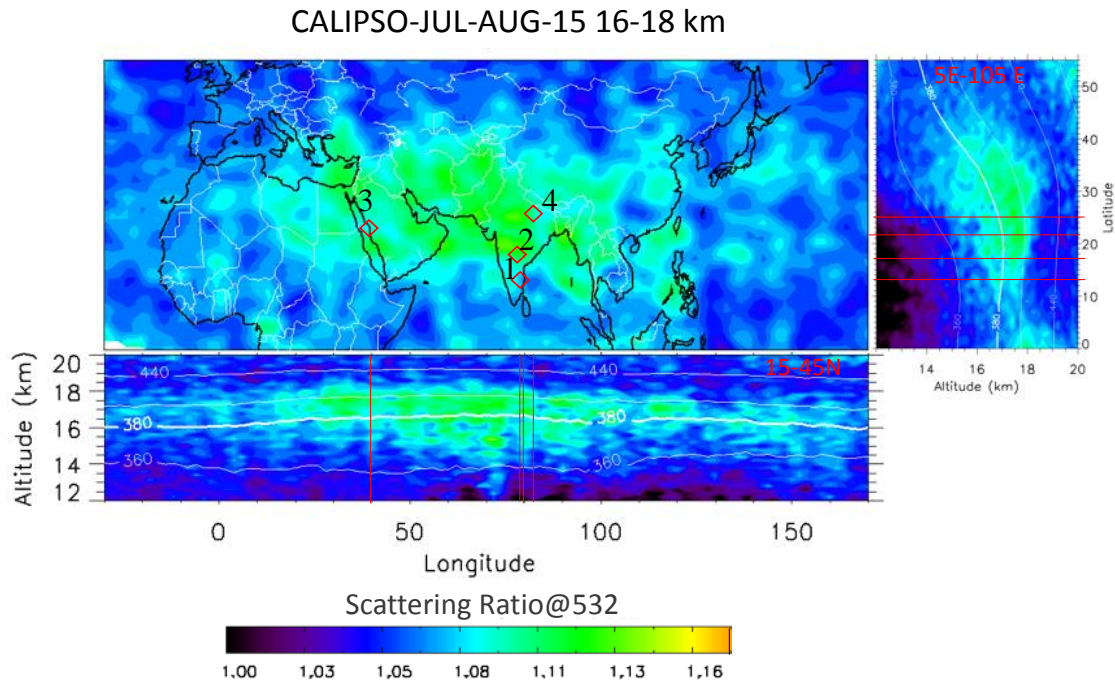
1
2
3
4
5
6
7
8
9
10
11
12
13
14
15
16
17
18

Figure 5. Time evolution of the GPS altitude four zero-pressure balloon flights on August 10th 2015, August 8th, 15th and 21st 2017.



1
2
3
4
5
6
7
8
9
10
11
12
13
14
15

Figure 6. Concentrations of carbon monoxide (CO), sulfate, nitrate, and black carbon (BC) at 100 hPa on 21 UTC, August 3, 2017, as predicted by the NASA GEOS-5 Forward Processing (FP) forecasting system on 00 UTC, July 30, 2017. Arrows denote winds. White dots along the white line (G and H) indicate two balloon sounding locations, Gadanki and Hyderabad, respectively.



1

2 *Figure 7. Map of Scattering Ratio (SR) at 532 nm after averaging the CALIPSO cloud-*
 3 *cleared data between 16-18 km in Jul-August 2015. Corresponding cross-sections from*
 4 *averaged data between 15°N-45°N (bottom) and 5°E-105°E (right) depict the 3-D extension*
 5 *of the ATAL. The white lines show isopleths of potential temperature (K). The locations of the*
 6 *balloon launches during the BATAL deployments are shown by red diamonds on the map and*
 7 *red lines on the cross-section. [1. Gadanki, 2. Hyderabad, 3. Thuwal, 4. Varanasi].*

8

9

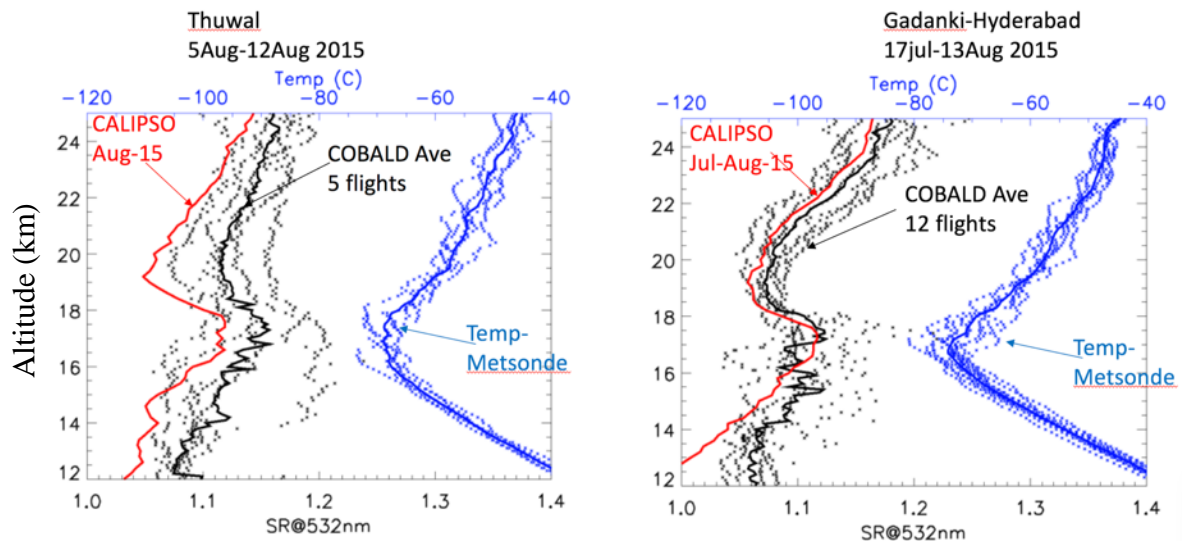
10

11

12

13

14



1

2 *Figure 8. SR profiles (black stars) at 532 nm derived from the COBALD balloon flights in*
 3 *Thuwal between 5-12 August 2015 (left) and Gadanki-Hyderabad between 17 July and 13*
 4 *August 2015 (right). Averaged COBALD profiles (black line) and CALIPSO profiles (red*
 5 *line) within $\pm 5^\circ$ latitude and $\pm 30^\circ$ longitude are shown. Radiosonde individual (blue*
 6 *stars) and averaged (blue line) temperature profiles are also shown.*

7

8

9

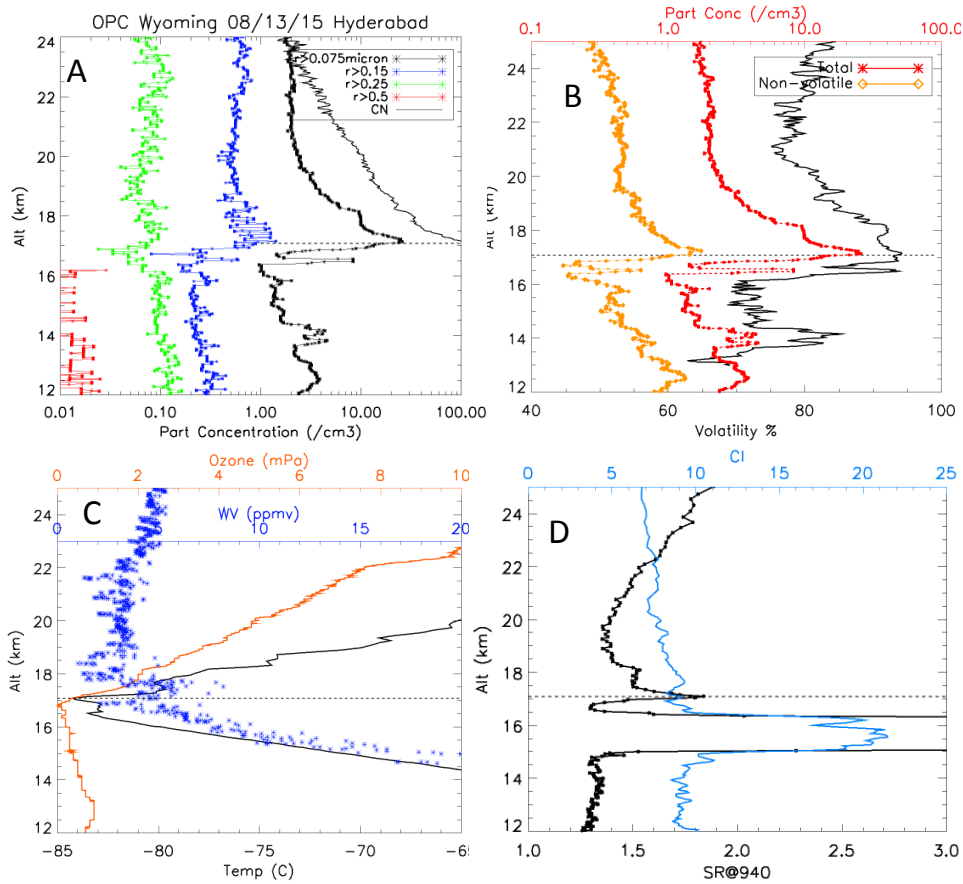
10

11

12

13

14



1

2 *Figure 9. Heavy balloon flight ascent profile of data collected on August 13th, 2015 from*

3 *Hyderabad. (A) Particle Number Concentration (PNC) profiles from unheated Optical Particle*

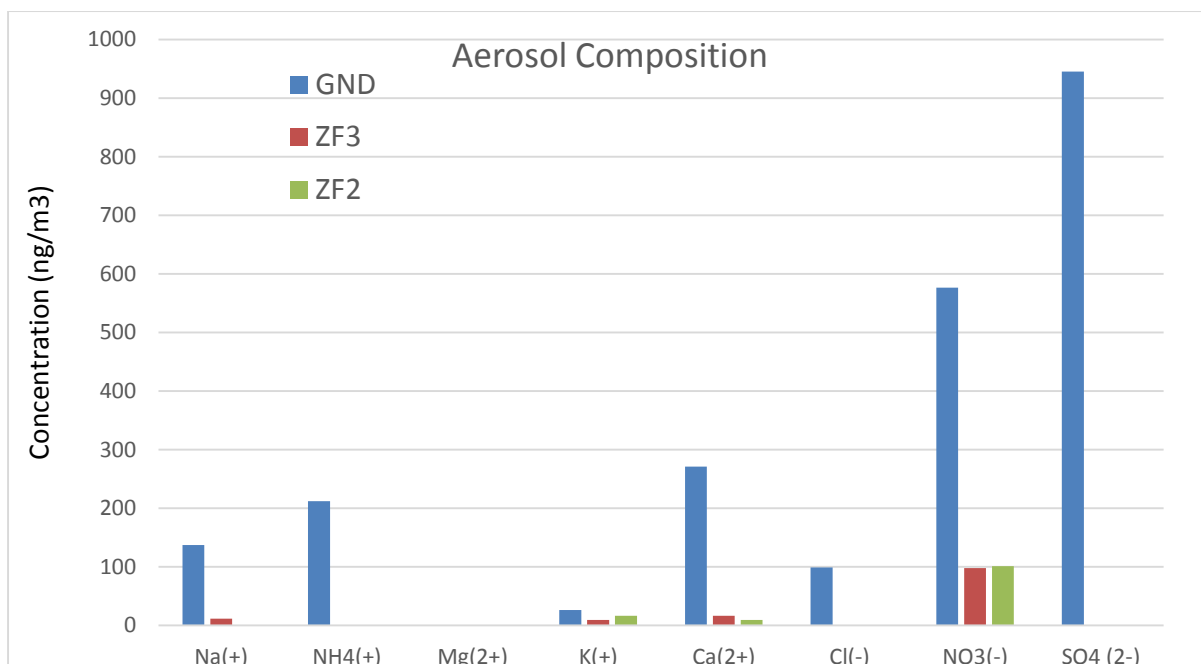
4 *Counter (OPC) for radius: $r > 0.075$, > 0.15 , > 0.25 , > 0.5 μm and Condensation Nuclei (CN)*

5 *profile. (B) PNC profiles for $r > 0.075$ μm from heated (180°C) and unheated OPCs. (C)*

6 *Temperature, ozone partial pressure and water vapor mixing ratio profiles. (D) SR at 940 nm*

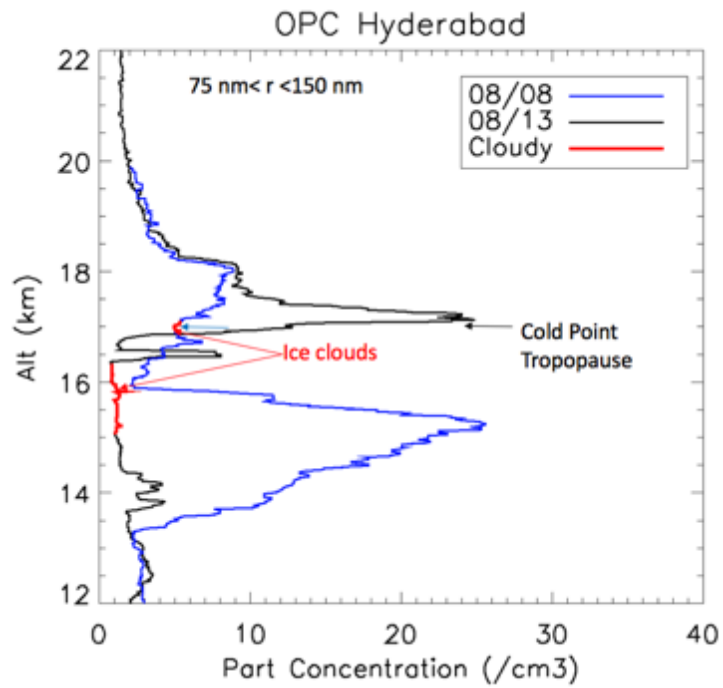
7 *and Color Index ($CI = (SR_{940} - 1) / (SR_{455} - 1)$) profiles from COBALD.*

8



1
 2 *Figure 10. Cations and anions concentration obtained from Ion Chromatography analysis to*
 3 *derive the composition of aerosols collected on board ZF2, ZF3 and on the ground (GND)*
 4 *during the 2017 BATAL campaign.*

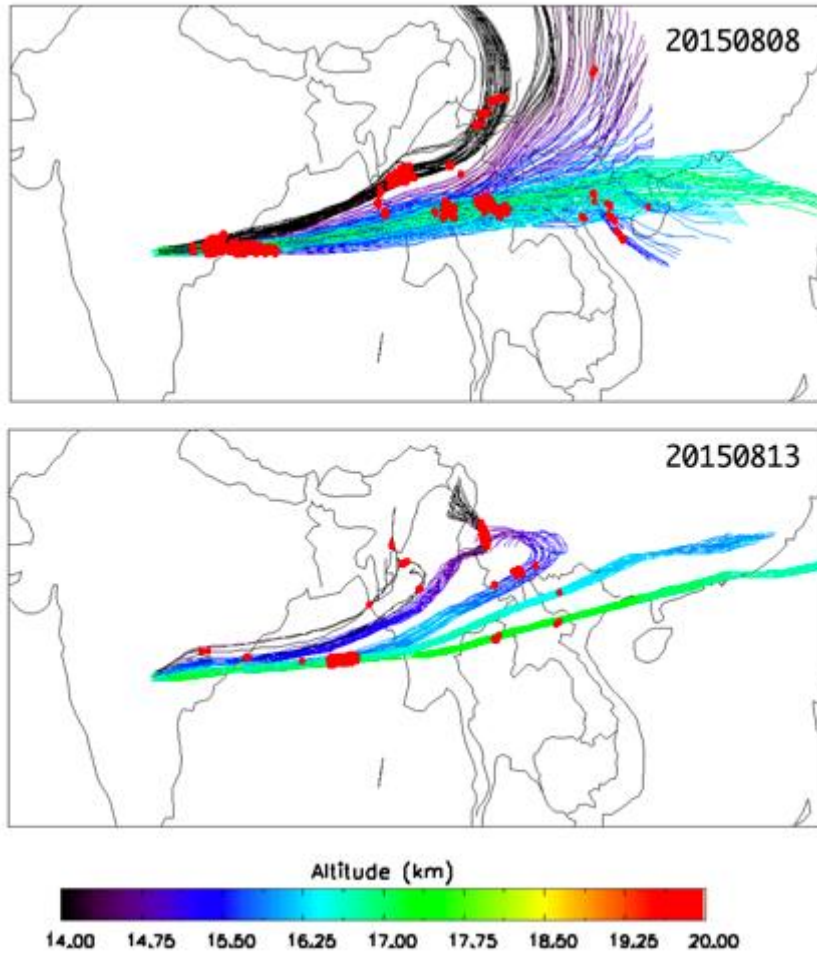
5
 6
 7
 8
 9
 10



1

2 *Figure 11. Aerosol concentration profiles for particles within $0.075 \mu\text{m} < r < 0.15 \mu\text{m}$ from*
 3 *the 2015 heavy balloon flights on 08/08 and 08/13 in Hyderabad. Part of the profiles where*
 4 *COBALD detected ice clouds based upon the Color Index(CI) is colored in Red. We note that*
 5 *the CI profile below 15 km on 08/08 was too noisy to apply the CI criteria.*

6



1

2 *Figure 12. Back trajectories initialized from the balloon flights on 08/13/2015 (top) and*
 3 *08/08/2015 (bottom) from Hyderabad. Red dots along these trajectories correspond to the*
 4 *presence of convection reaching the upper troposphere as seen by the HIMAWARI-8*
 5 *geostationary satellite.*

6

7

8

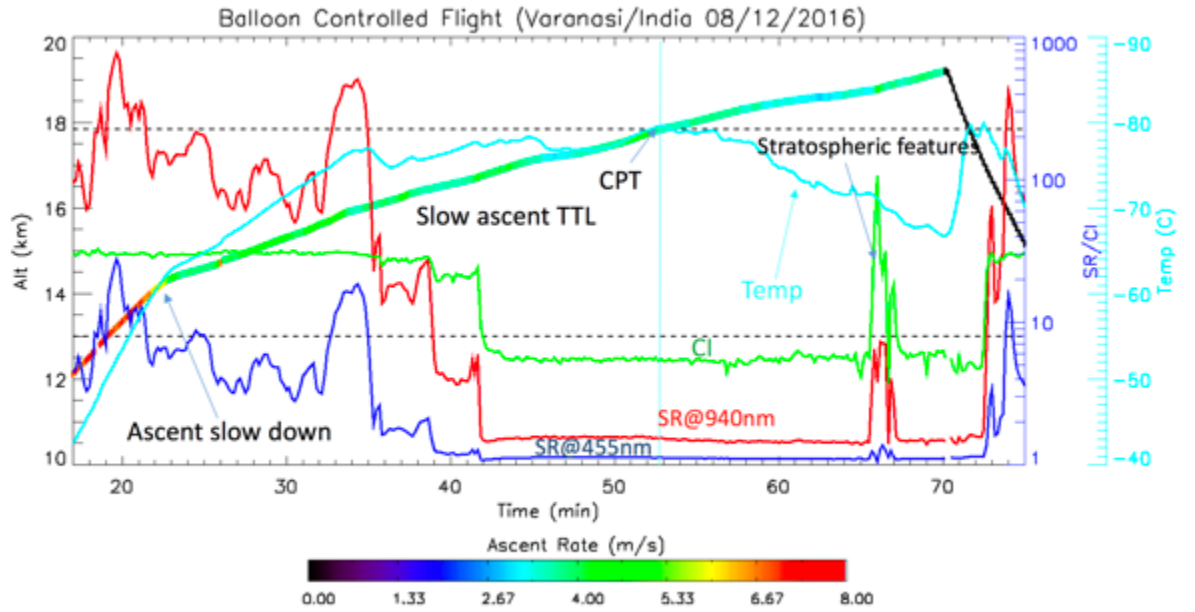
9

10

11

12

1



2

3 *Figure 13. (Top) Altitude, temperature, scattering ratios at 455nm and 940 nm and Color*
4 *Index (CI) time series along the Boomerang flight launched from Varanasi on 08/12/2016.*

5

6

7

8

9

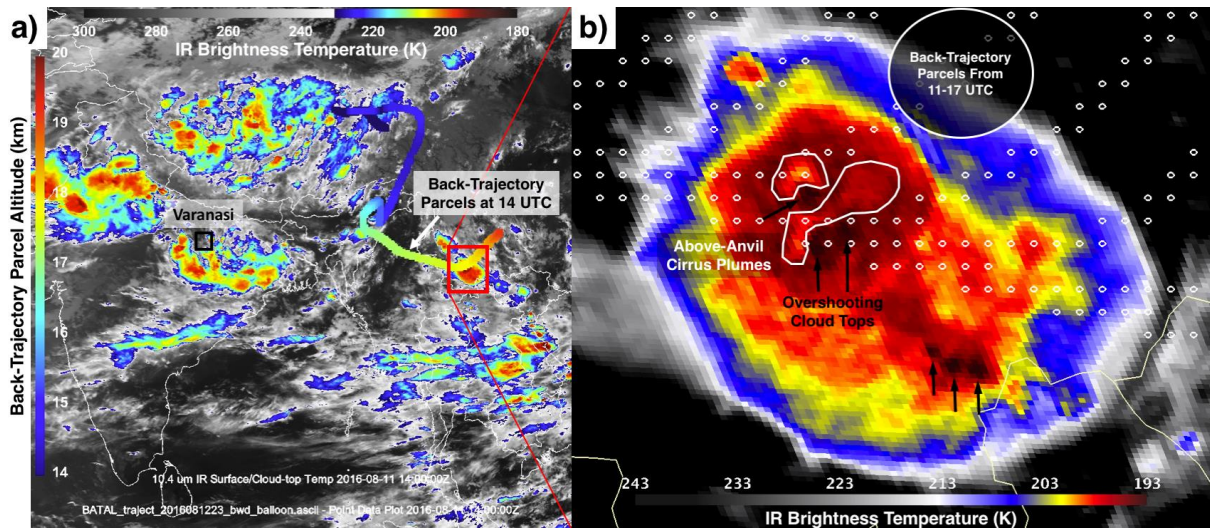
10

11

12

13

14



1

2 *Figure 14. (a) A Himawari-8 10.4 micron brightness temperature image at 1400 UTC on 11*
 3 *August 2016 over Southeast Asia. Back-trajectory air parcels at the time of the image,*
 4 *initialized from balloon flight position launched from Varanasi (India) 32 hours after,*
 5 *colored by their altitude, are overlaid. (b) A zoomed image at 1410 UTC over the region*
 6 *outlined by the red box in panel (a), contrast enhanced to more clearly show overshooting*
 7 *cloud tops (black arrows) and above-anvil cirrus plumes (white outline), embedded within*
 8 *the anvil of this mesoscale convective system. The locations of back-trajectory parcels above*
 9 *17.5 km from 11-17 UTC are overlaid with white circles, illustrating the uncertainty in parcel*
 10 *position at the time of the satellite image.*

11

12

13